Examining the Permeation of Toxic Chemicals Through Barrier Materials

Alex Bicket

Thesis submitted to the University of Ottawa
in partial Fulfillment of the requirements for the
Masters degree in Chemical Engineering

Department of Chemical and Biological Engineering
Faculty of Engineering
University of Ottawa

Abstract

The wide usage and availability of hazardous substances in many facets of todays life necessitate people must be in close proximity to, and risk contact with, hazardous chemicals during the conduct of their work. One layer of risk mitigation for exposure to hazardous substances is the use of protective equipment. In the case of hazardous chemicals, this is often a polymer layer worn to balance protection with mobility. However, modelling of the diffusion of chemicals through rubbery polymers is difficult and common test methods may contain sources of error inherent in the experimental design. Through numerical simulations, this thesis examines the accuracy of current standard test methods, seeks to determine which factors have the most impact on errors and suggests mitigations. Experiments were conducted to examine the permeation and determine transfer properties using the time-lag method. This work suggests that some common testing protocols have sources of error inherent to the design and experimental conditions must be carefully considered when selecting test protocols.

Contents

List of Figures

List of Tables

Legend

A	Surface area of a membrane
C	External concentration of liquid on a membrane surface
CF	Coverage fraction, the ratio of surface area covered in permeate to the total surface area of the membrane
$c_{i,1}$	Concentration of species i at point 1
D	Intrinsic Diffusivity
D_{eff}	Effective Diffusivity
J_i	Flux of species i
L	Thickness of a membrane
LCt_{50}	Lethal Concentration for 50% of a given population
LD_{50}	Lethal Dose for 50% of a given population
m	Mass
P	Permeability Coefficient
r	Radial coordinates
R	Radius of membrane and droplet radius of permeate on a membrane
R	Ideal gas constant
S	Solubility
t	Time
T	Temperature
V_m	Molar Volume of the Permeate
V_p	Permeate Volume
z	Axial coordinates
α	Receding factor, used to represent the rate of change of droplet radius
ϕ	Angular coordinates
θ	Time lag

Acknowledgements

I would like to thank my thesis supervisor, Dr Jules Thibault, for his patient guidance and help developing ideas into this work. I would also like to thank Dr Vivian Lau of Defence Research and Development Canada for her conduct of experiments, expert advice, and encouragement along the way. Without their help, I would have been unable to complete this work and learn as much as I did.

For her enthusiasm in helping me write, my daughter Elizabeth and my wife, Anarosa, for giving me the time to work on this.

Statement of Contributions

This work has not been submitted or accepted for any other degree. Dr Jules Thibault and Dr Vivian Lau supervised and co-authored the papers that form the main body of this thesis.

The responsibilities of the author (Alex Bicket) were:

1 To conduct a literature review of the field of chemical personal protective equipment (PPE) and the related fields of membrane science and CBRN defence to provide background material for the thesis.
2 To design experiments both in numerical simulation and laboratory to examine how certain variables impact the transport properties calculated from various experimental designs.
3 To analyze, interpret and visualise the data from the simulations and experiments and draw conclusions from the data.
4 To use the results of the experiments to recommend experimental methods and suggest ways to correct experimental error.
5 To produce the papers forming the main body of this thesis
6 To write a paper-based thesis to partially meet the requirements of a Master of Applied Science in Chemical Engineering from Ottawa University.

Chapter 1 - Introduction

This thesis is written as a thesis by articles. The main body consists of two chapters prepared as papers for publication on the topic of the permeation of liquids through rubbery polymer membranes. The thesis examines current experimental protocols for testing diffusion through non-porous polymer membranes such as those commonly used as protective materials. This thesis examines possible experimental error through the simulation of experiments and the conduct of actual experiments to better understand how liquids move through polymer membranes and how experimental conditions impact the results of the experiments, and how those experimental results should be interpreted. In this thesis, we have chosen the context of dermal hazards posed by persistent classes of nerve agents. This generally represents a liquid contact hazard and can remain present in the environment for long periods, and emphasis will be placed on topics specifically relevant to these hazards.

1.1 Background

1.1.1 Definition and types of Chemical Weapons

The Chemical Weapons Convention (CWC) defines Chemical Weapons (CW) as "(a) Toxic chemicals and their precursors, except where intended for purposes not prohibited under this Convention, as long as the types and quantities are consistent with such purposes; (b) Munitions and devices, specifically designed to cause death or other harm through the toxic properties of those toxic chemicals specified in subparagraph (a), which would be released as a result of the employment of such munitions and devices; and (c) Any equipment specifically designed for use directly in connection with the employment of munitions and devices specified in subparagraph (b)."[1] With toxic chemicals defined as "Any chemical which through its chemical action on life processes can cause death, temporary incapacitation or permanent harm to humans or animals. This includes all such chemicals, regardless of their origin or methods of production, and regardless of whether they are produced in facilities, in munitions or elsewhere."[1] A broad definition which can cover a large amount of the chemicals used for legitimate purposes today. However, in human history, and continuing to the current day, compounds have been developed

for the explicit purpose of causing death and harm to human beings for the purpose of killing on an industrial scale as nation states sought more powerful and deadlier weapons. Figure 1.1 shows the chemical structures of some of the most common CWA agents. These agents have been selected to provide examples that are relevant to this work as well as to show the different classes of CW.

(a)

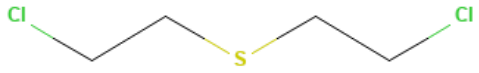

(b)

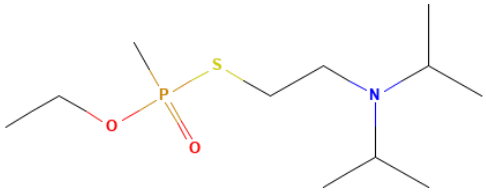

(c)

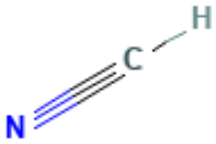

(d)

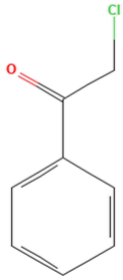

(e)

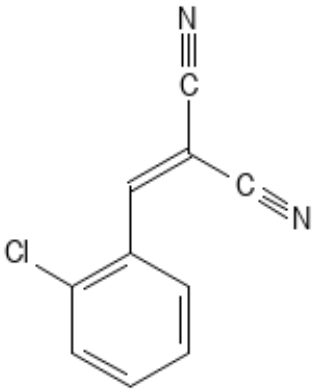

(f)

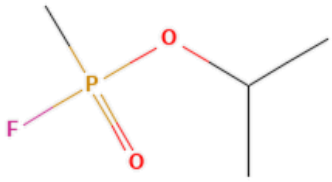

(g)

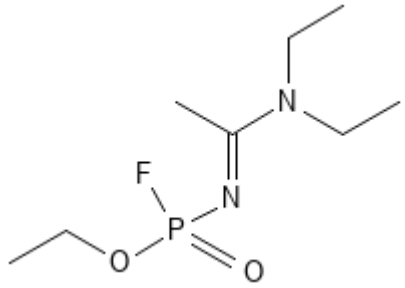

(h)

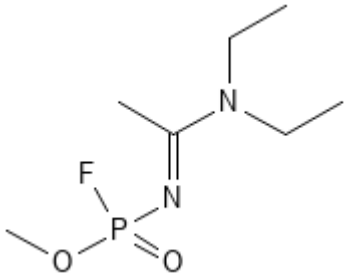

(i)

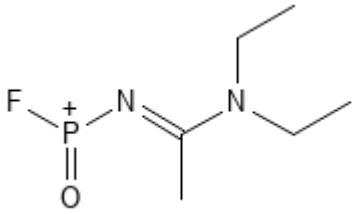

Figure 1.1: Chemical Structures of selected CWA (a) Sulphur Mustard (Bis(2-chloroethyl) sulfide)[2] (b) VX (O-Ethyl S-(2-diisopropylaminoethyl) methylphosphonothioate) (c) Zyklon-B (hydrogen cyanide)[3], (d) Tear Gas (2-Chloroacetophenone)[4], (e) CS Gas (2-Chlorobenzylidenemalononitrile)[5], (f) Sarin (2-[fluoro(methyl)phosphoryl]oxypropane)[6] (g) Novichok A-230[7], (h) A-232[8] and (i) A-234[9].

The Organisation for the Prohibition of Chemical Weapons (OPCW) recognizes 5 types of Chemical Agents: Choking Agents (such as chlorine gas), Blister Agents (such as sulphur mustard), Blood Agents (such as Zyklon-B), Nerve Agents (such as VX, Sarin and the Novichok series) and Riot Control Agents (such as Tear Gas and CS Gas)[10].

1.1.2 Toxic Mechanisms of Chemical Weapons

Chemical Weapons and any hazardous chemical can have a wide variety of effects on the human body. The exact effect and mechanisms of the effect tend to vary by the individual chemical. The CWC has divided CW into 5 distinct classes based on the broader mechanisms of action[1]. Choking Agents, such as chlorine gas and phosgene, are chemicals whose effects damage lung or respiratory

tissue when inhaled. When sufficient amounts of choking agent are inhaled, they inhibit gas exchange within the lungs preventing sufficient oxygen from entering the bloodstream[11]. Blister Agents, such as Sulphur Mustard, cause direct damage to any surfaces they come into contact with. The chemical mechanisms of damage vary by chemical and are described in more detail by Schwenk[11]. In general, blister agents are corrosive to tissue and cause inflammation, blisters, cellular damage and DNA damage to the exposed tissue[2,11,12]. When they are lethal, it is typically through damage to the airways or organ failure. Blood Agents are agents which inhibit cellular respiration, either through preventing the transport of oxygen in the blood or inhibiting the transfer of oxygen from the bloodstream to the cells[3,11,13]. Riot Control Agents are generally non-lethal and cause irritation, pain and inflammation in the eyes, mouth, throat, skin, and lungs on contact. They are intended to temporarily incapacitate affected persons, unlike other classes of agents described and are far more prolific around the world[4,5,11].

Nerve Agents are a class of CWA that target the nervous system. They represent the most toxic and lethal class of CWA (see Table 1.1). When an organophosphate nerve agent infiltrates the human body, it inhibits the cholinesterase enzymes, obstructing the breakdown of acetylcholine. As a result, this neurotransmitter accumulates excessively, leading to disruptive effects on the nervous system[14,15]. This has a wide variety of effects on the human body which can be broadly categorized in three ways: muscarinic effects, nicotinic effects and Central Nervous System (CNS) effects. While varied, it leads to death when exposure to enough nerve agent occurs. Death is caused by respiratory failure due to muscular weakness[14,15]. As toxic doses of nerve agents are frequently very low (see Table 1.1 which shows the Lethal Dose for 50% of the population (LD_{50}) and the Lethal Concentration for 50% of the population (LCt_{50}) of selected Chemical Agents through different exposure methods), the hazard posed by contact with even minute amounts of nerve agent is often extreme. Exact lethal doses are difficult to predict as human experiments would be extremely unethical and impossible to conduct safely. Simulation or animal modelling is typically used to predict doses. Further, even at sub-toxic doses of such agents, it is suggested that chronic issues may plague survivors of chemical agent poisoning past the immediate recovery period[14]. Further, casualties caused by a chemical agent can pose a hazard to anyone trying to help affected individuals without the appropriate protective equipment. The nerve agent may remain on the outside of the body or clothing, posing a vapour and liquid contact hazard as well as

contaminated tissue, vapour contamination in a casualty's breath or contaminated bodily fluids all posing a potential hazard[16].

Table 1.1. Lethal doses for various CWA in humans

Agent	**LD_{50} (Oral) [mg/kg]**	**LD_{50} (Dermal, liquid) [mg/kg]**	**LCt_{50} (Inhalation) [mg-min/m^3]**
GA (Tabun)		14 - 21[14]	135-150[14]
GB (Sarin)		24[14] 28[6]	70[14]
VX	0.10[17]	0.04 – 0.14[14]	30[14]
A-232	0.57[17]		
A-234	0.71[17]		
Sulphur Mustard	0.7[18]	100[18]	1500[18]
HCN			2032 - 20632[18]
Chlorine			13500[18]
Phosgene			1500[18]

1.1.3 Personal Protective Equipment (PPE)

The risk of toxic chemical absorption through the skin necessitated the development of protective measures to safeguard against chemical weapons, complementing existing respiratory protection[19]. Materials science has been able to provide better protective materials to personnel who may be exposed to CWA the need to balance protection from the hazardous chemical with the risk caused by burdensome protective equipment, such as overheating or loss of dexterity preventing the completion of necessary work[20]. This means that PPE must be carefully selected based on the agent, possible routes of exposure, the amount of time that personnel may be exposed, and the nature of work in the hot zone they are required to undertake. Depending on the level of protection required, a PPE ensemble will likely consist of respiratory protection, a protective suit, protective gloves, and protective boots[20]. Normally, gloves and boots will be made from a flexible, but permeation-resistant polymer such as butyl rubber, while suits can be multi-layered with an outer

liquid-resistant layer and an inner activated carbon layer for vapour protection[20]. However, the correct choice of PPE requires an understanding of how the chemical in question interacts with the material.

1.1.4 History of Chemical Weapons and Recent Uses

On 22 April 1915, to begin the second battle of Ypres, the German Army released chlorine gas as a weapon against French and Canadian positions. This use marked the first major use of toxic chemicals as a weapon in human history[21,22] and was followed by continued use and development of Chemical Weapons (CW), which would eventually cause around a million casualties during the First World War[22]. In July of 1917, the German Army employed sulphur mustard (bis (2-chloroethyl) sulfide) as a weapon, which could be absorbed through the skin as well as the lungs, necessitating the development of skin protection in addition to respiratory protection[19] to protect people against these threats. In the 1930's, German scientists developed the first organophosphate pesticides, compounds which act on the nervous system by inhibiting Acetylcholinesterase (AChE) receptors[23], in parallel Germany developed the first nerve agents, tabun and sarin[19,24]. After the Second World War, many of the victorious countries used the information captured from the Germans to establish their own chemical warfare programs and continued to develop Organophosphate nerve agents. Most notably, Venomous Agent X (VX) was developed in the 1950s by the British and entered industrial production in the 1960s[19]. VX has a lower vapour pressure than other commonly used Chemical Warfare Agents (CWA) and thus is an example of the class of persistent agents[25]. Persistent agents can remain as liquids in the environment for significant periods of time either on surfaces or absorbed into materials[26]. Due to their ability to permeate skin, extremely low lethal dose (see Table 1.1) and low vapour pressure pose a liquid contact hazard to any person who is around an area contaminated by them[14].

While the usage of CW became much less common after the First World War, governments have continued to employ them as weapons of war or against their own populations as well as widespread use of less acutely toxic, but still dangerous, compounds in huge amounts as insecticides, particularly dangerous as many of the most effective insecticides were not selective about inhibiting insect AChE or that of the human agriculture workers using them[24]. Historical examples of CW usage include the use of tear and mustard gas by Italy in Ethiopia in the 1930s,

the use of Zyklon B in concentration camps by Germany during the Holocaust, the use of mustard gas by Egypt in Yemen in the 1960s, the use of CS gas (2-Chlorobenzylidenemalononitrile) by American and South Vietnamese forces in the Vietnam War, the use of sulphur mustard and nerve agents by Iraq in the Iran-Iraq war of the 1980's and on the Iraqi Kurdish population in the late 1980s[19]. The non-state use of CW has been limited, however Aum Shinrikyo used sarin several times in Japan in 1996[19] and Islamic State used CW in both Syria and Iraq between 2015 and 2017[27,28] demonstrating that the capability to create and employ CW is not limited to state governments and parties to the Chemical Weapons Convention (CWC).

Due to their horrific nature and potential for causing mass death, treaties or agreements trying to limit the use of chemical or poisonous weapons have a long history. The Strasbourg Agreement of 1675, between France and Germany to limit the use of poison bullets, is the first international agreement of this type. In 1874, the Brussels Convention on the Law and Customs of War proposed limits on the use of poison and poisoned weapons. In 1899, the Hague Peace Conference (and the second one in 1907) sought to place similar limits on the worlds militaries[19,29]. The evidence of WW1 shows these treaties had little to no impact. In 1925 the international community tried again by implementing the Geneva Protocol, which once again, seems to not have stopped very many nations from employing them when they wanted to[19]. The current international treaty banning the use of chemical weapons is called the Chemical Weapons Convention (CWC), negotiations began in the 1970s but a treaty would not enter into effect until 1997. With the entry into effect of the CWC, the Organisation for the Prohibition of Chemical Weapons (OPCW) was created[29]. To date, the Chemical Weapons Convention has 193 States Parties, along with one signatory state and three states that have not signed the agreement. The OPCW claims 100% of the world's declared stockpiles of chemical weapons have been destroyed, and the OPCW continues to conduct regular inspections of state stockpiles and industrial facilities which produce precursors or could be repurposed to produce chemical weapons[30]. However, recent uses of chemical weapons continue despite the widespread adoption of the CWC. This necessitates the maintenance of capabilities that can manage and respond to incidents involving CW release and continued research into the detection of and protection against such hazardous chemicals.

In recent years, contemporary use of chemical warfare agents has been seen in Syria, Great Britain, Malaysia, Russia, and Iraq by various agents of state governments and non-state organisations.

Several examples of their use by authoritarian regimes have taken place in the last ten years, either as a method of assassinating dissidents or other persons who displeased the regime or as a weapon intended to inflict terror on a population. These uses have been described in further detail in the news and by the OPCW's fact-finding missions and technical assistance visits. These incidents include the murder of Kim Jong-Nam at Kuala Lumpur International Airport in Malaysia using VX[31–33]; attacks on Syrian citizens by the Syrian Arab Army in the Syrian Civil War[27,34,35,35–39]; the use of chemical weapons by Islamic State in both Iraq and Syria[27,28]; the attempted murder of Sergei Skripal by Russian Agents in Salisbury, UK in 2016, which resulted in the death of an unconnected woman and several injuries[40–49]; and the attempted murder of Russian opposition politician Alexei Navalny[50–52]. Of particular interest were the use of novel, previously little-known, chemical warfare agents known as "Novichoks" in the attempts on Mr. Skripal and Mr. Navalny's lives. These chemicals were a class of persistent Nerve Agent developed by the Soviet Union towards the end of the cold war and were relatively unknown[47,53–55]. Due to the limited amount of knowledge of these chemicals, the cleanup attempts and initial response to the Salisbury incident were quite challenging as the agents were difficult to detect and it was unknown how they interacted with protective equipment[43,44].

1.1.5 Permeation Testing Methods, Standards, and Relevant Theory

Typical permeation testing methods for protection against liquid hazards are described in a summary paper by Banaee and Que Hee[56] and in US Army TOP 08-2-501A[57], with the differences between the two (complete coverage of the membrane vs droplets used to achieve a specific dose) being important to this work. Previous work done by Rivin et al.[58] has compared test methods and shown that the method using individual droplets may not provide accurate steady state permeability or diffusivity values, thereby leading to errors if those test results are used to predict the transport properties of a system. Both of these test methods use the time lag method[59,60] to calculate the effective diffusivity by extrapolating the steady state slope of the plot of the total accumulated quantity having permeated through the membrane as a function of time to the time-axis using Equation (1.1).

$$\theta = \frac{L}{6D_{eff}} \tag{1.1}$$

Once the time lag is determined, we can use the slope of that same plot of the accumulated quantity to calculate the permeability P of the system using the Equation (1.2)[61], adapted from equations used for gas permeability by using the liquid concentration instead of the feed gas pressure, substituted as in liquid or incompressible systems where the driving force is not a pressure gradient but a concentration gradient. Similarly, the total mass of the studied chemical permeated through the protective material is used instead of the change in the gas pressure on the downstream side of the membrane.

$$P = \frac{dm}{dt}\frac{L}{A\,\Delta C} \tag{1.2}$$

In this case, P is measured in m^2/s. The change in mass or moles over time should be in the same units as the concentration – mass or moles per unit volume.

The solution diffusion theory describes the diffusion of molecules through non-porous polymer membranes[62]. As non-crystalline polymers do not have a uniform or "still" molecular structure, the molecules within the polymer matrix undergo Brownian motion. As these molecules move, void spaces are created within the matrix of the polymer which molecules of the permeating chemical can occupy and move through. Given sufficient time within the matrix, a molecule trapped in one of the void spaces within the polymer structure is highly likely to traverse the entire membrane thickness. This can occur either by the void space linking with another, enabling the molecule to shift, or through the void space itself randomly migrating within the polymer matrix. Eventually, the void may open to the opposite side of the membrane, allowing the permeate molecule to diffuse outward after successfully penetrating the material[63]. In this way, it is possible for substances to diffuse through a material even though there is no complete porous path from one side of the material to the other. Materials with rigid crystalline structures have much lower permeabilities, as there is little to no random motion of molecules forming the crystalline structure[63]. In solution diffusion theory, we can use Equation (1.3) to describe the permeability (P) of a substance through a membrane as the product of diffusivity and solubility.

$$P = DS \tag{1.3}$$

While there are pores in "non-porous" membranes, formed by the spaces between polymer chains and branches, they are sufficiently small to not allow the majority of molecules to diffuse through them, with the gaps being less than 5 – 10 Å[63]. This means that the permeability of molecules in the membrane is not described by pore flow and is only governed by the solubility of the permeate in the membrane itself and molecular diffusion. Further, the driving force of diffusion of this type is limited to that driven by concentration gradients (or partial pressure of gases) and not by other factors. Fick's law of diffusion describes this diffusion (with some limitations around swollen membranes and multi-component systems)[64]. The second form of Equation (1.4) is defined using the external concentration of permeate at the surfaces of the membrane.

$$J_i = -D_i\left(\frac{dc_i}{dz}\right) \; or \; J_i = -D_i S_i\left(\frac{dC_i}{dz}\right) \tag{1.4}$$

This equation becomes much more complicated to solve in three-dimensional cases requiring partial differential equations to solve to examine diffusion in all directions. When these equations are combined with the time-lag theory, it is possible to determine the transport properties of a system using experimental or simulated data and calculate a mass balance across the membrane allowing its characterization.

1.1.6 Focus of this investigation

In this thesis, the focus has been placed on liquids with low vapour pressure, representative of the persistent class of CWA. The interactions of vapours with protective equipment are much better understood, and the hazards associated with agents that evaporate, and thus dissipate, more quickly can be mitigated in different ways. However, agents with low vapour pressures can persist in the environment much longer and are thus more likely to have the route of exposure be through direct contact with a liquid. The interaction between chemical vapours and filter materials, either those used in air purifying respirators or suits lined with a filter media, is better understood than the interactions between liquid contaminants and barrier materials and is simpler to test. Due to the complexities of molecular diffusion, it is more difficult to predict or model the interactions between a liquid and a rubbery polymer membrane intended to protect someone from contact with that liquid. As the selection of appropriate PPE and the correct management of risk is dependent

on the system of hazard and protective material and understanding the interactions between the two, it presents an interesting challenge trying to better understand how the tests and the systems themselves may work and how we can reduce or simplify the requirements for physical testing by better understanding the systems and their interactions.

1.2 Thesis Subject

This thesis discusses the simulation of diffusion properties of liquid-polymer membrane systems to gain a deeper understanding in the evaluation of the experimental errors in common diffusion testing protocol specific to protective equipment for CBRN applications.

1.2.1 First Article: Simulating the Permeation of Toxic Chemicals through Barrier Materials

The first article of this thesis describes a series of numerical simulations of the permeation of liquids through rubbery polymer membranes. The simulations examined the variability of the results, and possible errors for a wide range of factors: (1) properties of the membrane such as the thickness, type of material (represented by diffusivity of the permeant in the material), and (2) the properties of the permeant, including the diffusivity of the permeant, the fraction of surface area of the membrane covered by permeant and the pattern or geometry of that surface area coverage. The simulations were used to examine the impact of these variables on the values of the transport properties calculated using the time-lag method and to suggest a possible method for correcting them, as well as the magnitude of values causing the significant effect.

1.2.2 Second Article: Experimental Examination of the Permeation of Chemicals Through Common Protective Materials.

The second article uses the results of solubility and permeation experiments conducted at DRDC to examine the relationships between surface area coverage and experimental error proposed in the first paper as well as to suggest methods of curve fitting to predict transport properties of the experimental system by comparing multiple methods, namely the time-lag method and non-linear regression methods using either two variables or a single variable to fit a curve to the experimental data points available.

1.3 Thesis Structure

This thesis is presented in four chapters. An introduction chapter that discusses the context of the work and provides a brief overview of the concepts examined in the next two chapters. The main body of the work consists of a paper that has been published in a scientific journal and a shorter chapter discussing experimental results, which will form the basis for a future paper. The final chapter is a more general discussion of the conclusions of the two main chapters and their possible implications.

Chapter 2 - Simulating the Permeation of Toxic Chemicals through Barrier Materials

Alex Bicket[1], Vivian Lau[2] and Jules Thibault[1]

[1]Department of Chemical and Biological Engineering, University of Ottawa, Ottawa, ON K1N 6N5, Canada; Jules.Thibault@uottawa.ca

[2]Defence Research and Development Canada, Ralston, AB T1A 8K6, Canada; vivian.lau@drdc-rddc.gc.ca

Abstract: Chemical warfare agents that are liquids with low vapor pressure pose a contact hazard to anyone who encounters them. Personal protective equipment (PPE) is utilized to ensure safe interaction with these agents. A commonly used method to characterize the permeability of PPE towards chemical weapons is to apply droplets of the liquid agent to the surface of the material and measure for chemical breakthrough. However, this method could produce errors in the estimated values of the transport properties. In this paper, we solved numerically the three-dimensional cylindrical Fick's second law of diffusion for a liquid permeating through a non-porous rubbery membrane to determine the time the permeating species will emerge on the other side of the polymer membrane. Simulations of different amounts of surface area coverage and the geometries of permeate on the membrane surface indicated that incomplete surface area coverage affects the estimation of the transport properties, making the experimentally determined transport properties unsuitable for predictive use. We simulated different permeation values to determine the factors that most influenced the estimation error and if the error was consistent over different permeate–membrane combinations. Finally, a method to correct the experimentally determined permeability is suggested.

Keywords: personal protective equipment; Fickian diffusion; numerical simulation; liquid coverage pattern; material properties

2.1. Introduction

When a hazardous chemical is released, it often requires people to access the area and put themselves at risk of exposure to the hazard to rescue injured people, investigate the event and its impact, or conduct a clean-up of the hazardous contamination. Elastomeric membranes are used as barrier materials in personal protective equipment (PPE) to protect against skin contact with toxic chemicals, including chemical warfare agents[65]. Non-porous rubbery polymers such as nitrile rubber, silicone rubber, and butyl rubber are common PPE materials, especially for gloves[66] where their flexibility gives the wearer dexterity while still being afforded a good degree of protection. In addition to functional properties, such as flexibility and weight, barrier materials are selected based on their chemical resistance, which is evaluated by measuring breakthrough, permeation, and degradation of the material when exposed to chemicals of interest[65]. Breakthrough time is one measure of how well a given barrier will protect against a chemical hazard, measuring the time it takes a chemical to completely permeate through the material[67], and is used to rate how long a piece of protective equipment will protect the wearer against that chemical.

However, transport properties are difficult to predict and are reliant on the individual system (permeate, membrane, and temperature), requiring physical experiments to derive the protective properties of the materials. In the case of diffusion through non-porous polymer membranes, the solution diffusion model is used to describe the motion of molecules of the permeate into and through the membrane[62,63,68]. Experimental procedures such as those described by ASTM F739, ASTM D6978, EN 374, EN 16523, ISO 6529, or US Army TOP 08-2-501A[56,57] are used to characterize the permeation of liquids through protective materials and determine transport properties in combination with the time-lag method of determining diffusivity using the steady-state flux of permeate through a membrane, as described by Dalton, Frisch and others[57,59,60,63].

Test methods used to evaluate PPE materials for chemical warfare defense applications involve placing individual droplets of a chemical agent on a circular sample of the test fabric and sampling the clean side of the membrane to detect the breakthrough of the chemical[57,58]. These tests can be resource-intensive and difficult to perform with highly toxic chemical permeates. However, simulation of the diffusion of molecules through dense polymer membranes is computationally intensive and difficult to use to predict transport properties[63,69].

An alternative approach is to apply experimentally obtained transport properties to computational models of membrane permeation. However, the experimentally obtained transport properties measured in standardized tests may not be appropriate. Rivin et al.[58] suggested that test methods using droplets of chemical permeant produce errors in the estimation of the transport properties derived through such testing suspected to be caused by the system not reaching steady-state diffusion or leading to transport properties different from those that would be obtained in the case of flooded permeation cells. Indeed, in this work, it is shown that transport properties obtained from experiments with partial coverage of the test membrane may be inaccurate. As a result, transport properties obtained from such experiments need to be interpreted with caution when used for PPE selection to protect against hazardous chemicals.

The objective of this study is to perform a series of numerical experiments to assess the impact of a partially covered membrane surface on the estimation of the membrane transport properties determined using the time-lag method. The impacts of partial coverage were assessed in conjunction with changing membrane thickness, changing the diffusivity of the permeate in the membrane, and changing the coverage geometry of the permeate on the surface of the membrane. The motivation for using partial membrane coverage is to minimize the amount of toxic liquid used in a permeation experiment. It is anticipated that the series of numerical simulations will allow us to find a correction factor that could be used to recover the actual membrane transport properties from those obtained experimentally. With a good estimate of the transport properties, the numerical model could then be used to examine various permeation scenarios.

2.2. Materials and Methods

2.2.1. Experimental Permeation System

The numerical experiments performed in this investigation are designed to model a typical diffusion cell for testing the permeation of hazardous chemicals[56–58,70]. A circular membrane swatch of the test membrane material is used and permeate is applied to one side of the membrane. As the permeate diffuses through the membrane, the amount of permeate found on the receptor side is quantified as a function of time to determine the transport properties of the membrane. The numerical experiments conducted were used to simulate the permeation of liquids through non-porous polymer membranes. Figure 4 shows a representative diffusion cell which is used to

determine experimentally the transport properties of the liquid moving across a membrane[56–58,70,71].

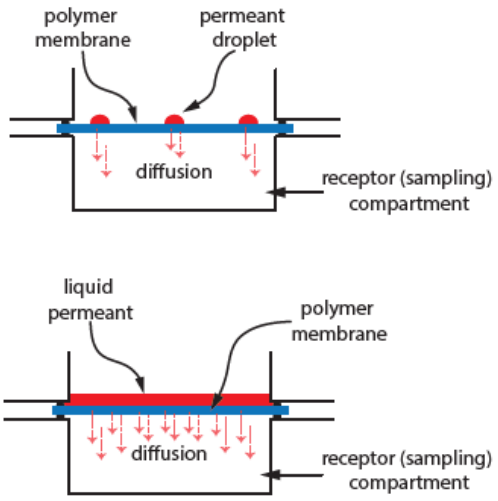

Figure 2.1. Simplified diffusion cell diagram depicting chemical permeant placed as droplets (top) or as flooded cell (bottom).

2.2.2. Numerical Simulations

In this investigation, the three-dimensional Fick's second law of diffusion Equation (2.1) was solved by finite differences using a program, written in Fortran programming language, developed by the authors for this application to determine the rate of permeation through a cylindrical dense membrane (Figure 2.2a), as typically incorporated within a permeation cell.

$$\frac{\partial c}{\partial t} = D\left[\frac{\partial^2 c}{\partial z^2} + \frac{\partial^2 c}{\partial r^2} + \frac{1}{r}\frac{\partial c}{\partial r} + \frac{1}{r^2}\frac{\partial^2 c}{\partial \phi^2}\right] \tag{2.1}$$

Equation (2.1) may be reduced to a one-dimensional partial differential equation in the permeation direction z when the feed side of the membrane is completely flooded. When the feed side of the membrane is partially covered, the three-dimensional diffusion equation must usually be solved. In this investigation, the finite difference in the three-directional mass transfer equation will always be solved to determine the temporal variation in the concentration within the membrane.

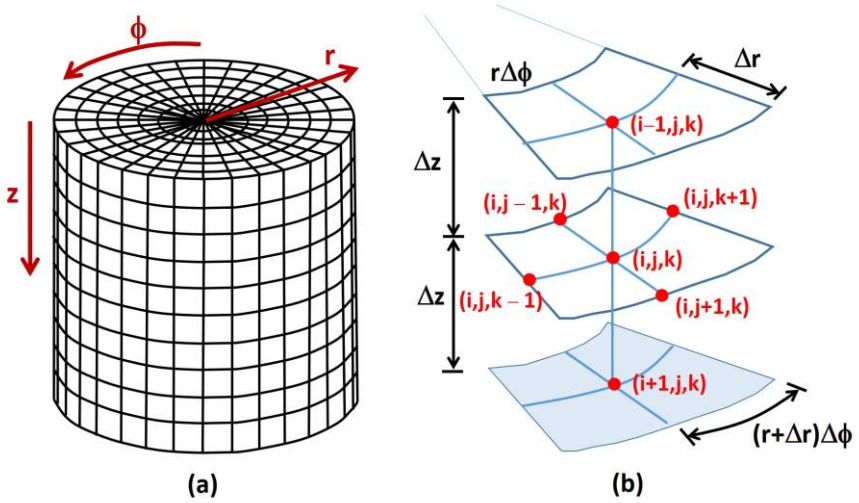

Figure 2.2. Discretized three-dimensional cylindrical membrane: (a) schematic diagram of a discretized membrane, and (b) central mesh point with its six neighboring mesh points used in Equation (2).

Equation (2.1) was discretized into a sufficiently large number of mesh points to generate small three-dimensional elements as shown in Figure 2.2b to achieve mesh independence. The discretized equation for a central mesh point is given in Equation (2.2) in its explicit form.

$$\frac{c_{i,j,k}^{t+\Delta t} - c_{i,j,k}^{t}}{\Delta t} = D\left[\begin{array}{l} \dfrac{c_{i-1,j,k}^{t} - 2c_{i,j,k}^{t} + c_{i+1,j,k}^{t}}{\Delta z^2} + \\ \dfrac{c_{i,j-1,k}^{t} - 2c_{i,j,k}^{t} + c_{i,j+1,k}^{t}}{\Delta r^2} + \dfrac{1}{(j-1)\Delta r}\dfrac{c_{i,j+1,k}^{t} - c_{i,j-1,k}^{t}}{2\Delta r} \\ + \dfrac{1}{((j-1)\Delta r)^2}\dfrac{c_{i,j,k-1}^{t} - 2c_{i,j,k}^{t} + c_{i,j,k+1}^{t}}{\Delta \phi^2} \end{array}\right] \tag{2.2}$$

The indices (i,j,k) refer to (z,r,ϕ) directions divided into (NI,NJ,NK) meshes. This equation calculates the internal concentration $c_{i,j,k}$ at mesh point (i,j,k) at the next time step Δt, i.e., at time $t + \Delta t$, based on the concentration at mesh point (i,j,k) and its six neighboring mesh points (Figure 2.2b) at time t. Equation (2.2) is valid for all internal mesh points describing the membrane. It is assumed that the dense membrane is isotropic, implying the membrane has a uniform composition structure throughout with constant diffusivity D and solubility S. In addition, it is assumed that the diffusivity and solubility are not functions of concentration and the system is isothermal.

To completely define the problem, it is necessary to provide the initial condition and six boundary conditions, two for each dimension. It is assumed that initially, the concentration of the migrating species throughout the membrane is zero (Equation ((2.3)).

$$\text{At } t = 0, \qquad c_{i,j,k}^{t=0} = 0 \qquad \forall i, j, k \tag{2.3}$$

At time zero, the liquid permeating species is added to the top surface of the membrane where it progressively dissolves into the dense membrane and migrates to the permeate side. The boundary conditions for the *z*-direction are given in Equations (2.4) and (2.5). Equation (2.4) simply states that the species concentration (*c*) at the top surface within the membrane is in instantaneous equilibrium with the concentration (*C*) of the liquid coverage outside the membrane. *S* is the membrane solubility of the migrating species. Equation (2.5) assumes that the concentration of permeate at the surface of the membrane on the receptor side is zero or close to zero. While this will not be strictly the case, we can assume that in a permeation cell where a liquid receptor solution is used instead of a sweep gas, the solvent has a high enough affinity for the permeate that the concentration at the membrane surface is equivalent to the concentration of permeate in the bulk solvent. In a diffusion cell where the permeant is sampled on the receptor side as a vapor, a constant gas flow is used to carry the permeant vapor to the detector[58]. As the rates of diffusion in the modeled system are generally very low and the levels of permeate that indicate breakthrough are generally very small, then the assumption is still valid.

$$\text{At } z = 0, \qquad c_{i=1,j,k}^{t} = SC_{i=1,j,k}^{t} \qquad \forall j, k \tag{2.4}$$

$$\text{At } z = L, \qquad c_{i=NI,j,k}^{t} = 0 \qquad \forall j, k \tag{2.5}$$

The boundary conditions for the radial direction are given in Equations (2.6) and (2.7). Equation (2.6) states that symmetry prevails at the center ($r = 0$) of the membrane. The second term in the *r*-direction of Equation (2.1) is undetermined at the center since both the partial derivative and the radius are both equal to zero. However, using L'Hôpital's rule, this term is easily equated to the second partial derivative concerning *r* and the radial term can be easily discretized. It is important to note that for the symmetry condition at the center of the membrane to prevail, the liquid must be distributed symmetrically on the surface of the membrane, especially when a multiple-drop

pattern is used. Equation (2.7) simply states that at the outside circumference of the membrane, an impermeability condition prevails.

$$\text{At } r = 0, \qquad \frac{\partial c^{t}_{i,j=1,k}}{\partial r} = 0 \qquad \forall i,k \tag{2.6}$$

$$\text{At } r = R, \qquad \frac{\partial c^{t}_{i,NJ,k}}{\partial r} = 0 \qquad \forall i,k \tag{2.7}$$

The boundary conditions for the angular direction (ϕ) are given in Equations (2.8) and (2.9). Both boundary conditions assumed symmetry at ϕ equal to zero and some other angle where symmetry prevails. This angle could be 2π if symmetry does not prevail at a smaller angle. In this investigation, $\pi/2$ and 2π were used depending on the case study. One particular aspect of the angular term of Equation (2.1) is the singularity at the center point of the membrane. Few techniques have been proposed to deal with this singularity[72]. In this investigation, at the center point (j = 1), the zero radius was replaced with 0.1% of the first radial mesh point Δr.

$$\text{At } \phi = 0, \qquad \frac{\partial c^{t}_{i,j,k=1}}{\partial \phi} = 0 \qquad \forall i,j \tag{2.8}$$

$$\text{At } \phi = \phi_1, \qquad \frac{\partial c^{t}_{i,j,k=NK}}{\partial \phi} = 0 \qquad \forall i,j \tag{2.9}$$

The average upstream and downstream fluxes were obtained from the concentration gradients at the upstream and downstream fluid–membrane interfaces using Equations (2.10) and (2.11). Convergence to the steady permeation rate was assumed to be reached when the average fluxes (J) at the upstream and downstream surfaces were the same, within 0.01%. The downstream average flux allows calculation of the rate of accumulation of the migrating species on the permeate side. Under steady state, the rate of accumulation becomes constant and the extrapolation to the time axis of the constant accumulation curve as a function of time provides the time lag (θ) from which the effective diffusivity can be determined, see Equation (2.12).

$$J_{z=0} = \frac{1}{\pi R^2} \int_0^R \int_0^{2\pi} -\mathrm{D} \left.\frac{\partial c}{\partial z}\right|_{z=0} r\,dr\,d\phi \qquad \text{(Upstream)} \tag{2.10}$$

$$J_{z=L} = \frac{1}{\pi R^2} \int_0^R \int_0^{2\pi} -D \left. \frac{\partial c}{\partial z} \right|_{z=L} r\,dr\,d\phi \quad \text{(Downstream)} \tag{2.11}$$

$$\theta = \frac{L^2}{6D_{eff}} \tag{2.12}$$

where R is the radius of the membrane, D_{eff} is the effective diffusivity of the migrating species in the membrane, and L is the membrane thickness. Note that an apparent or effective diffusivity (D_{eff}) has been used, Equation (2.12), instead of the intrinsic diffusivity (D) because the measured diffusivity via the time-lag method may not be equal to the intrinsic diffusivity in the case of an incomplete liquid coverage on the upstream surface of the membrane. It is important to stress that the intrinsic diffusivity of the membrane remains constant and is independent of the fraction of the liquid coverage. For complete liquid coverage, the measured diffusivity should be equal to the intrinsic diffusivity.

2.2.3. Different Liquid Patterns and Surface Area Coverage

In this paper, several cases are examined to determine which variables influenced the values of the transport properties calculated for partial coverage scenarios. The fraction of coverage of the feed surface area of the membrane was varied to examine and quantify previous work carried out by Rivin et al.[58] which suggested that incomplete coverage leads to errors in the determined transport properties. The simulation also examined if different patterns of permeate added to the membrane surface would impact these measurements. Several patterns with different drop sizes and geometries were simulated and labelled 1 to 4 as illustrated in Figure 2.3. The droplet patterns were adapted from the test patterns described in US Army TOP 08-2-501A[57] to a droplet pattern with radial symmetry. Other drop patterns were also investigated.

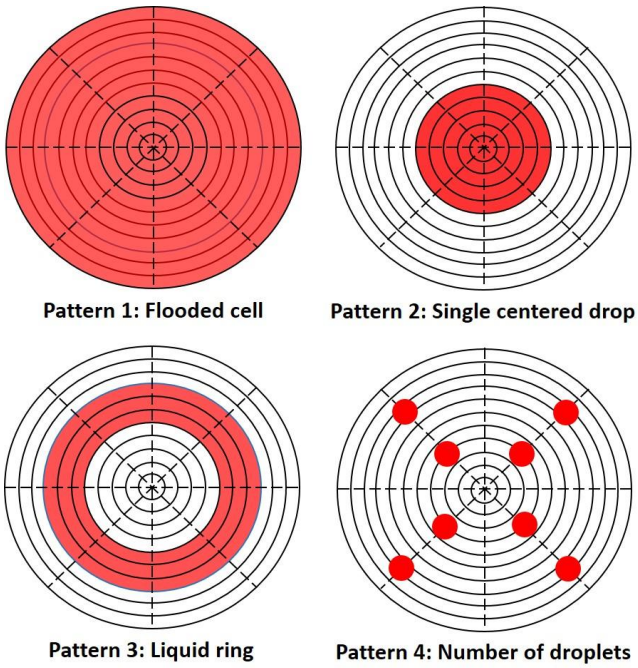

Figure 2.3. Examples of liquid patterns of the migrating species (in red) used at the membrane feed surface as boundary conditions for numerical experiments.

2.3. Results and Discussion

This section presents the simulation results for various case studies to examine the impact of various variables on the estimation of the membrane properties, namely the liquid coverage pattern, fraction surface coverage, membrane intrinsic properties, and membrane thickness. The results show that the membrane properties are estimated accurately, as expected, in the case of a flooded cell and these results will serve as a basis of comparison for the other case studies.

2.3.1. Validation of the Numerical Simulations

Before presenting the results of various numerical simulations, it is important to examine the accuracy of the numerical model with a known benchmark solution. Figure 2.4 shows the comparison between the analytical and numerical solutions for the case where the feed side of the membrane is completely flooded at time $t = 0$. It is the only benchmark solution that is available for this problem, which is reduced in this case to a one-dimensional solution. Equation (2.13) gives the analytical solution of the concentration profile $c(z,t)$ throughout the membrane as a function of time (t) and relative membrane thickness (z/L) for this case study. This analytical solution was

obtained by the method of separation of variables[73]. The results of performed. Figure clearly show that the numerical solution for the concentration profile as a function of time corresponds exactly to the analytical concentration profile. An overall mass balance evaluated the accuracy of the simulations in the case of the partial liquid coverage of the membrane. In all cases, the overall mass balance was shown to be very accurate.

$$c(z,t) = CS\left(1-\frac{z}{L}\right)-\left(\frac{2CS}{\pi}\right)\sum_{n=1}^{\infty}\left[\frac{1}{n}\sin\left(\frac{n\pi z}{L}\right)e^{-\left(\frac{Dn^2\pi^2 t}{L^2}\right)}\right] \tag{2.13}$$

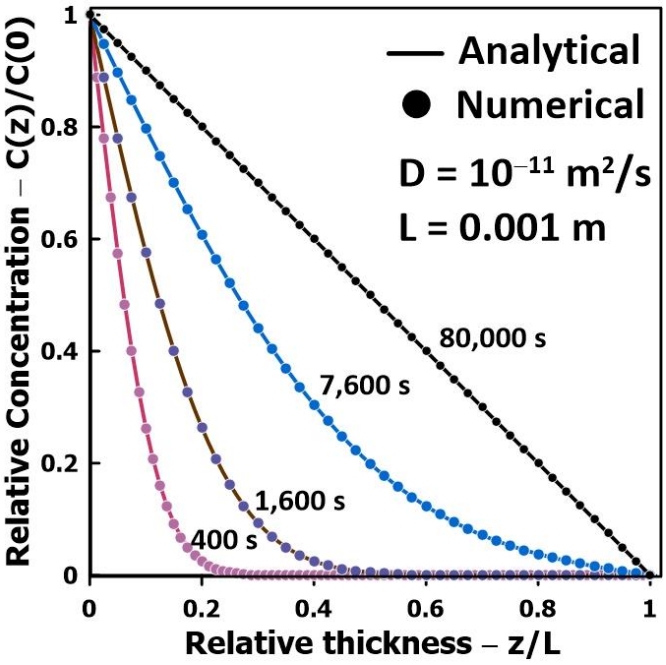

Figure 2.4. Comparison of analytical and numerical solutions in the case of one-dimensional diffusion occurring when flooded cell experiments are performed.

2.3.2. The Impact of the Membrane Diffusivity

To examine the impact of the membrane diffusivity (D) on the estimated effective diffusivity (D_{eff}) for different membrane thicknesses, a series of numerical experiments were conducted over a wide range of membrane diffusivity values and for a constant liquid fraction coverage. The estimated diffusivity was obtained with the time-lag method. The results of these numerical experiments are presented in Figure 2.5 and show that, for a constant membrane thickness, the estimated effective diffusivity is directly proportional to the actual membrane diffusivity as the ratio D_{eff}/D remains

constant over the whole range of diffusivity. On the other hand, the thickness of the membrane has a major impact on the diffusivity ratio. For thin membranes, the diffusivity ratio is close to unity and the estimated diffusivity is relatively well estimated, where it approaches the value that is obtained with a flooded cell. It is important to state that the actual diffusivity (D) of the membrane is independent of the coverage pattern, and it is the value that we are attempting to recover. However, because of the fractional liquid coverage, the three-dimensional species permeation leads to an estimated value, termed effective diffusivity (D_{eff}), that is different from the intrinsic membrane diffusivity.

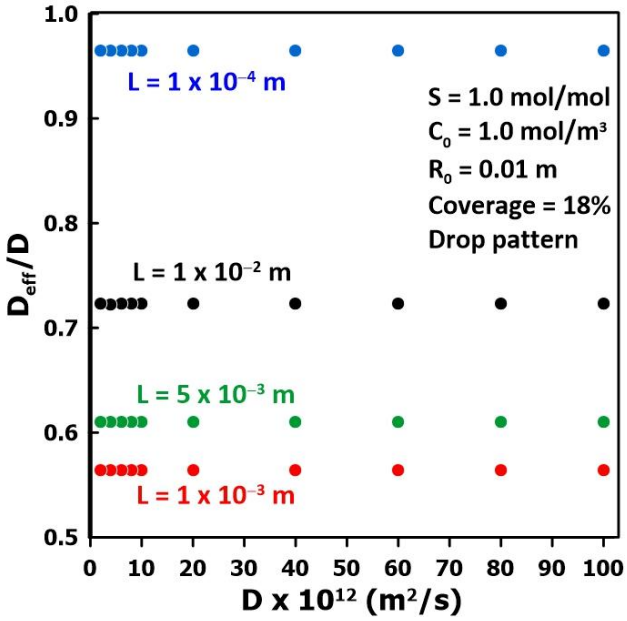

Figure 2.5. The ratio of the effective diffusivity and the actual diffusivity (D_{eff}/D) as a function of the membrane diffusivity for four different membrane thicknesses with constant fraction coverage (Pattern 4).

2.3.3. The Impact of Membrane Thickness

Figure 2.6 presents the results of a series of simulations to examine the impact of the membrane thickness on the estimation of the membrane diffusivity for a single drop of liquid centrally located on the membrane and covering 18% of the membrane surface. The results show that, as the thickness of the membrane increases, the difference between the effective diffusivity and the actual diffusivity increases over a wide range of thicknesses. The diffusivity ratio (D_{eff}/D) reaches a minimum at a thickness of approximately 6 mm with a relative diffusivity of approximately equal

to 0.55. At higher membrane thicknesses, the effective diffusivity starts to increase. It is hypothesized that the diffusivity ratio will asymptotically increase back to unity for a much larger, albeit unrealistic, membrane thickness. Similar trends were observed for all the partial coverage patterns tested and the local minimum was in the same order of magnitude. This minimum occurs at smaller thicknesses for smaller coverage areas. These numerical simulations demonstrate that a significant estimation error of the intrinsic diffusivity should be expected for some common protective equipment[20,74–76], given the typical thickness of these protective garments. These errors typically lead to an underestimation of the actual diffusivity for a given system.

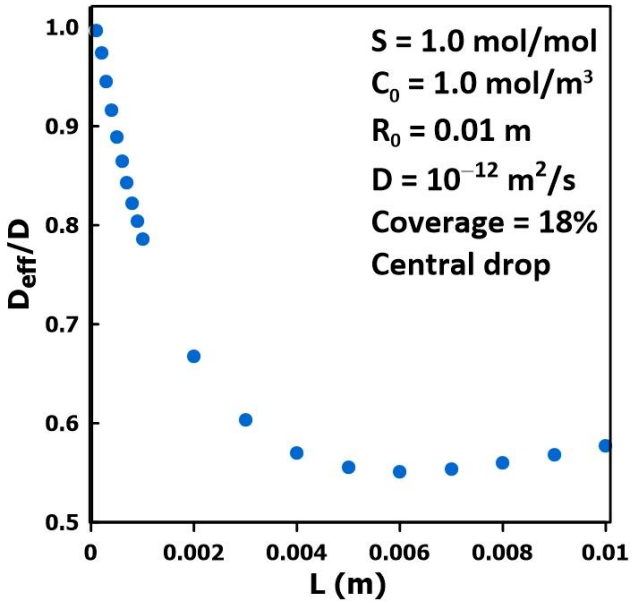

Figure 2.6. The diffusivity ratio (D_{eff}/D) as a function of the membrane thickness for a central liquid drop (pattern 2) covering 18% of the membrane surface.

To explore the reason for the observed minimum in the diffusivity ratio and its subsequent increase as the thickness increases, the radial concentration profiles under steady state were obtained at five different relative depths (z/L) within the membrane and are presented in Figure 2.7. These results were obtained for a centered droplet covering 30% of the membrane surface area. Figure 2.7a presents the concentration profiles for a very thin membrane, L = 100 µm, showing very negligible radial diffusion such that the inlet and exit permeation areas are nearly identical with a flat concentration profile. The membrane diffusivity is very well estimated, with a ratio of D_{eff}/D of 0.984. In Figure 2.7b, a larger radial diffusion was observed for a membrane having a thickness ten times larger (1.0 mm), which delayed the attainment of the steady state and the time lag. As a

result, the estimated diffusion coefficient is smaller than the actual diffusion coefficient with a diffusivity ratio D_{eff}/D of 0.809. When the membrane thickness is yet ten times larger (10 mm) and equal to the radius of the membrane, the migrating species have a significantly larger radial diffusion as shown in Figure 2.7c. The thickness is sufficiently large for the migrating species to diffuse to the impermeable diffusion cell boundary. As a result, a nearly flat concentration profile is observed close to the permeate side of the membrane. The estimated diffusion coefficient is smaller than the actual diffusion coefficient with a diffusivity ratio D_{eff}/D of 0.643. This data point for this relatively thick membrane is in the increasing portion of the D_{eff}/D versus L plot and further increasing the membrane thickness, although unrealistic, would lead to a relative diffusivity even closer to the actual diffusivity as a larger relative portion of the membrane reaches a flat concentration profile.

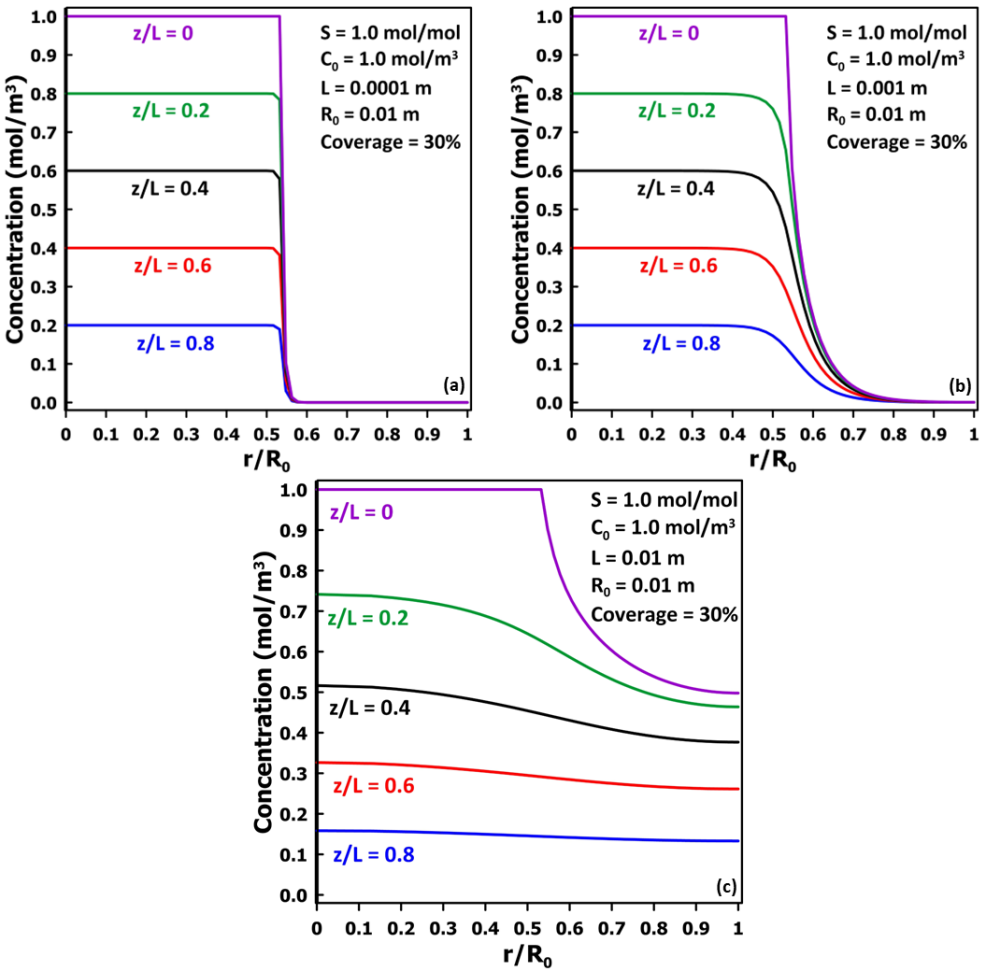

Figure 2.7. Concentration vs. r/R_0 at different values of z/L for a single-centered droplet for three membrane thicknesses: (a) 100 μm, (b) 1.0 mm, and (c) 10 mm.

2.3.4. The Impact of Permeate Geometry

Figure 2.8 presents the results of the series of simulations performed to examine the variation in the relative diffusivity as a function of the thickness for two different drop patterns covering 12% of the surface membrane area. The droplet diameter, the diffusivity, and the number of droplets were held constant while, as shown in the two insets of Figure 2.8, the location of the outer layer of droplets was changed. The results show that, for thin membranes, the relative diffusivity ratio is approaching unity. However, as the thickness of the membrane increases, the relative diffusivity decreases rapidly to reach a minimum at a thickness between 1 and 2 mm. For both drop patterns, the minimum value of the relative diffusivity is nearly the same with a value of approximately 0.51 and 0.49 for the droplet pattern with the outer ring, shown in red, closer to the center and for the droplet pattern with the outer ring, shown in blue, further from the center, respectively. Beyond the minimum value, the relative diffusivity increases more smoothly with an increase in thickness. Even though the relative diffusivity is affected by the distribution of droplets on the surface of the membrane, the main factors affecting the diffusivity estimated by the time-lag method remain the thickness of the membrane and the liquid fraction coverage.

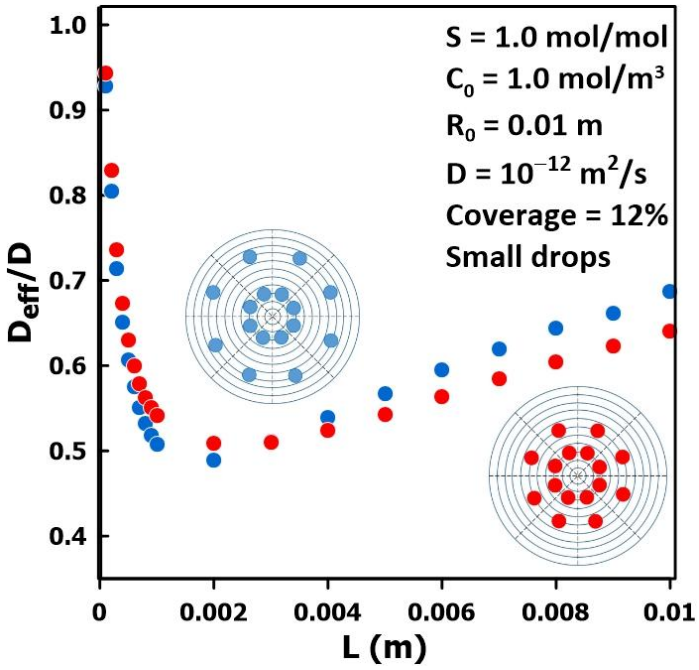

Figure 2.8. Diffusivity ratio D_{eff}/D as a function of the membrane thickness for two different drop patterns for a liquid surface coverage of 12%.

2.3.5. The Impact of Membrane Surface Area Covered by the Permeate

Figure 2.9 presents the results of a series of simulations performed to assess the variation in the relative diffusivity for two different liquid patterns, namely patterns 2 and 3, as a function of the surface coverage fraction. The results show that, as the fraction of the membrane surface covered by the liquid permeate increases, the relative diffusivity ratio approaches unity. Indeed, the intrinsic diffusivity of the membrane is obtained when the membrane surface is flooded by the liquid permeate. Results clearly show the effect of the liquid fraction coverage on the relative diffusivity as determined by the time-lag method. Both liquid patterns compared in this series of simulations are in close agreement with each other, suggesting that the effects of coverage are much less impacted by the geometry of the permeate on the membrane surface than the effects of thickness and the coverage fraction. Practically, in this case, as the fraction of the membrane covered by permeate increases, the patterns tested become increasingly similar.

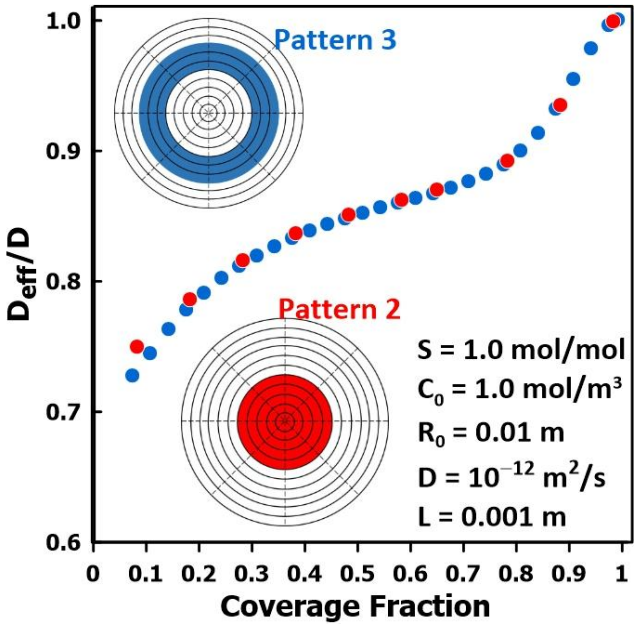

Figure 2.9. The ratio of the effective diffusivity over the actual diffusivity as a function of the liquid fraction coverage for Patterns 2 and 3.

Figure 2.10 shows a comparison of the relative diffusivity varying with the fractional coverage of the membrane surface for pattern 3 and four different membrane thicknesses. The results of Figure 2.10 clearly show the effects of both the coverage fraction and the membrane thickness for a constant coverage pattern. The value of the relative diffusivity D_{eff}/D asymptotically tends to unity

in all cases when the fraction coverage of the membrane surface area approaches unity, which is a flooded cell (pattern 1). These results corroborate the work of Rivin et al.[58] who state that the "flooded cell" scenario is the ideal method to estimate the intrinsic diffusivity of the membrane, as it corresponds to the case of one-dimensional diffusion.

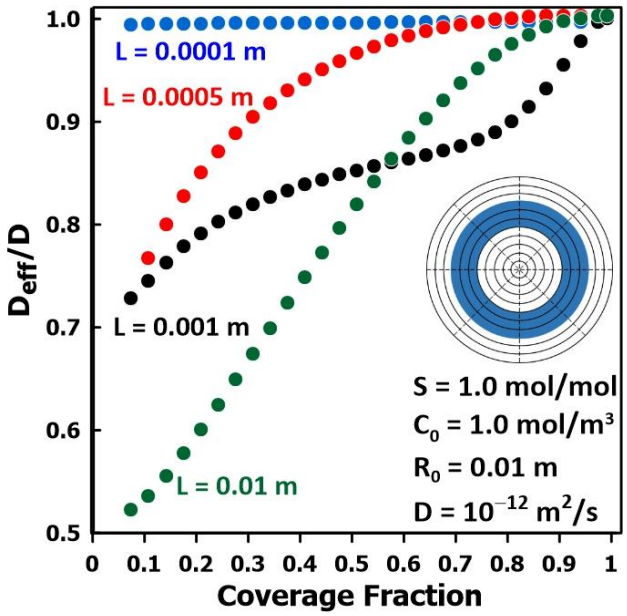

Figure 2.10. The ratio of the effective diffusivity over the actual diffusivity as a function of the coverage fraction for Pattern 3, for four different membrane thicknesses.

2.3.6. Receding Liquid Coverage

Previous results clearly show that with flooded cell experiments, the membrane diffusivity is estimated accurately, whereas, for partial liquid surface coverage, its estimation needs special attention. In addition, with partial coverage, the liquid coverage area may recede as a function of time because of permeant sorption and evaporation, thereby affecting the dynamic permeation rate. Indeed, the rate of recession of the liquid typically depends on the thickness of the liquid cover, the liquid surface tension, the rate of evaporation, and its diffusivity and solubility in the membrane. Figure 2.11 presents the comparison of the dynamic permeation results for an initial central circular liquid pattern for a 2 mm thick membrane. A series of simulations were performed with different exponential decays of the liquid coverage radius as expressed by Equation (2.14), with the radius R of the liquid cover decreasing from the initial liquid radius R_0 as a function of a receding factor α, time t, and time lag θ. The results shown in Figure 2.11 were obtained with an

initial radius of approximately 0.007 m and a receding factor of 0.05 chosen to examine a slowly receding liquid.

$$R = R_0 e^{-\alpha t/\theta} \tag{2.14}$$

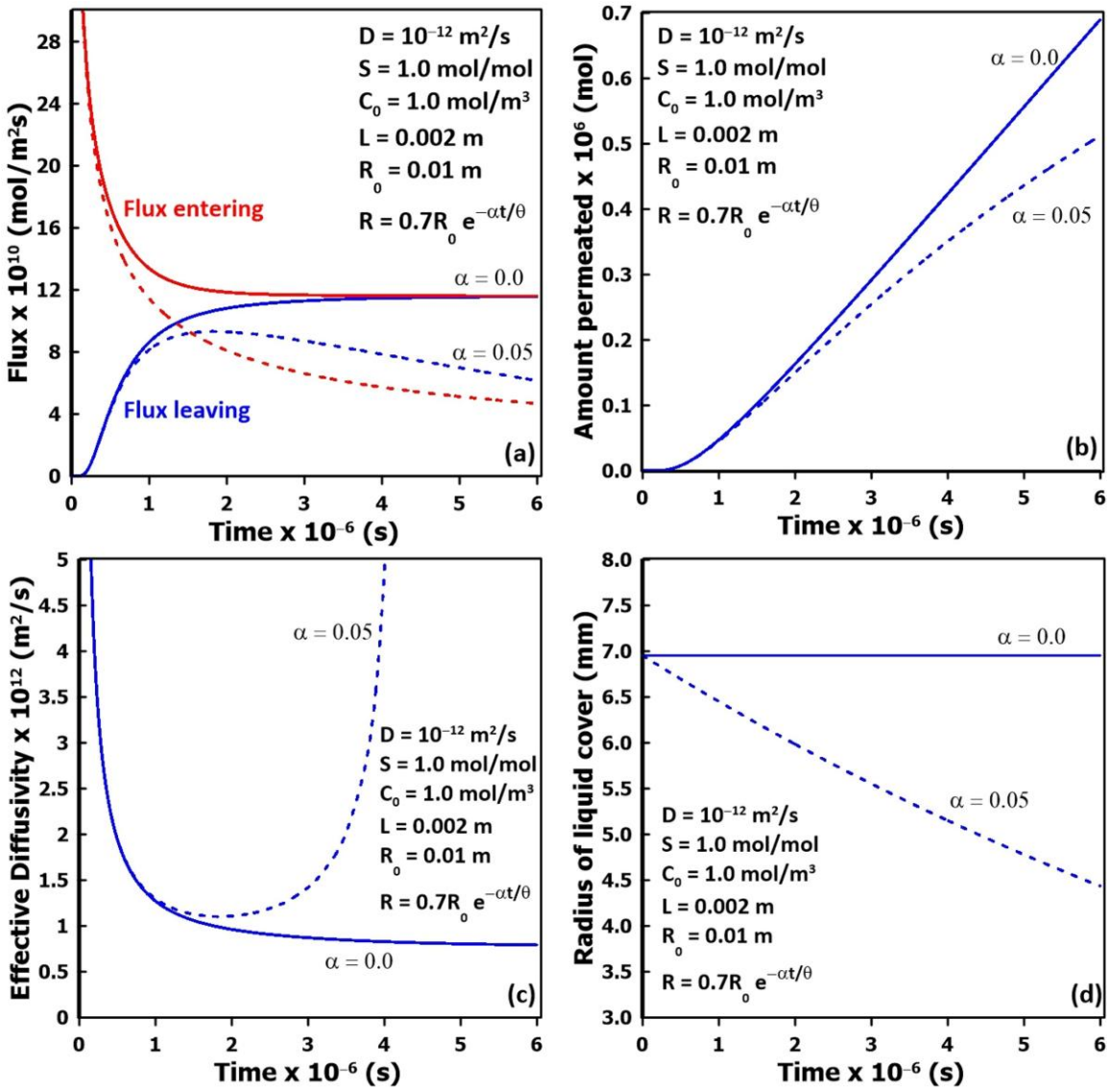

Figure 2.11. Comparison of the dynamic permeation results with (α = 0.05) and without (α = 0.0) receding liquid pattern: (**a**) upstream and downstream molar fluxes, (**b**) total amount permeated, (**c**) effective diffusivity estimated by the time-lag method, and (**d**) variation in the radius of the liquid coverage for the two receding factors.

Figure 2.11a presents the inlet and outlet average fluxes of the migrating species as a function of time through the membrane. For a constant liquid cover (α = 0), the two average fluxes

progressively become equal as they approach the steady state. When the liquid cover recedes as a function of time, as expected, the average fluxes become smaller than fluxes under constant coverage. For a longer permeation time, the liquid will completely disappear, and the two fluxes will eventually approach zero. For higher values of the receding factor, simulating higher diffusivities or lower vapor pressures, the average fluxes will decrease even faster. The corresponding amount of the migrating species that has permeated through the membrane is plotted in Figure 2.11b for the two values of the receding factor. For constant coverage, the rate of accumulation becomes relatively constant, and the time lag can be determined, while for receding coverage, the rate initially increases before progressively decreasing. For the latter case, it is more difficult to determine the time lag as the slope of the accumulation curve is never constant and does not entirely satisfy the underlying assumptions of the time-lag method. Figure 2.11c presents the estimation of the effective diffusivity determined from the instantaneous time lag as a function of time that was calculated from the slope of the plots of the accumulated amount that had permeated through the membrane (Figure 2.11b). In the case of constant liquid coverage, the instantaneous time lag progressively assumes a nearly constant value. A small decrease is still observed in Figure 2.11c because of the slow lateral diffusion that is required to reach a perfect steady state. For a receding liquid coverage, the instantaneous effective diffusivity initially decreases, then passes through a minimum before increasing again as a function of time. It is interesting to note that the minimum value of the effective diffusivity is very close to the actual value of the membrane diffusivity. In practice, a permeation experiment will probably last only for the first part of the curve when the concentration curve of the accumulated permeate would attain an almost linear trend, corresponding to an experimental time of between 1 and 2×10^6 s (Figure 2.11b) for this relatively thick membrane. Finally, Figure 2.11d presents the variation in the radius of the central liquid coverage as a function of time for both cases considered in this section.

In practice, in the case of a receding liquid coverage to use the synergy between the experimental and numerical determinations of the effective diffusivity, it would be necessary to take images of the feed surface pattern as a function of time. It will then be possible to estimate the intrinsic diffusivity of the migrating species within the tested membrane.

2.3.7. Predictive Model for the Estimation of the Diffusivity Ratio

The results of the previous sections have clearly shown that a partial liquid coverage on the surface of the membrane may lead to an incorrect estimation of the diffusion coefficient of the liquid being tested. Ideally, a complete surface coverage should be used whenever possible. However, in the case of a very toxic liquid, it is advisable to use a drop pattern distribution to minimize the quantity of liquid used. The results obtained in this investigation provide the necessary data to develop a model that could predict the diffusion coefficient ratio D_{eff}/D. The correction factor depends on numerous factors. Nevertheless, it is desired to find the simplest model that could provide an acceptable estimation of D_{eff}/D. Having determined the effective diffusion coefficient D_{eff} experimentally, the actual diffusion coefficient D can therefore be estimated.

In this investigation, an artificial neural network was used to estimate the diffusion coefficient ratio as a function of the two most important contributing factors: the thickness of the membrane and the coverage fraction. Artificial neural networks are now commonly used successfully for a myriad of engineering applications. The high degree of plasticity in its structure is the main reason for its ability to efficiently represent the underlying causal relationship between input and output data. In this investigation, a three-layer feedforward neural network (FFNN) was used to predict D_{eff}/D as a function of some input process variables. The FFNN is comprised of an input layer, a hidden layer, and an output layer, as shown in Figure 2.12. The input layer contains three neurons corresponding to the two independent variables plus the bias neuron. The two independent variables of Figure 2.12 are the scaled values of the logarithmic value of the membrane thickness and the liquid coverage fraction. The input information is simply transferred to the neurons of the hidden layer and the output layer. Appendix A provides the detailed development of the FFNN used to predict D_{eff}/D. The results of 797 numerical simulations were used to determine the weights of the FFNN by minimizing the sum of squares of the differences between the diffusivity ratio D_{eff}/D obtained numerically and the one predicted by the neural network. The 797 data points are comprised of 226 records for pattern 2, 254 for pattern 3, and 317 for pattern 4. Figure 2.13 presents the parity plot of the prediction of the diffusion coefficient ratio D_{eff}/D for three different liquid coverage patterns. The coefficient of regression R^2 is provided in Figure 2.13 for each liquid coverage pattern. The fit is not perfect since only the two main factors were considered as inputs to the model. The average relative error is 2.44% ± 2.36 and the maximum relative error is 15.4%.

It is believed that the prediction error of this model is acceptable and allows us to estimate with good accuracy the diffusion coefficient ratio D_{eff}/D.

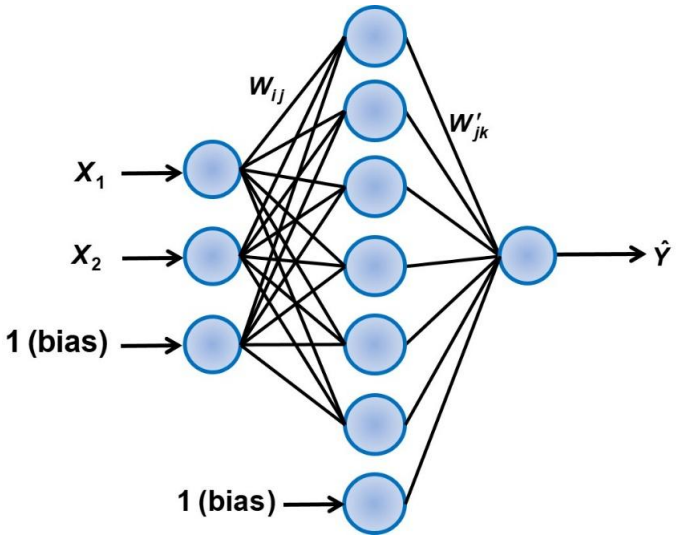

Figure 2.12. Feedforward neural network used for the estimation of the diffusion coefficient ratio D_{eff}/D.

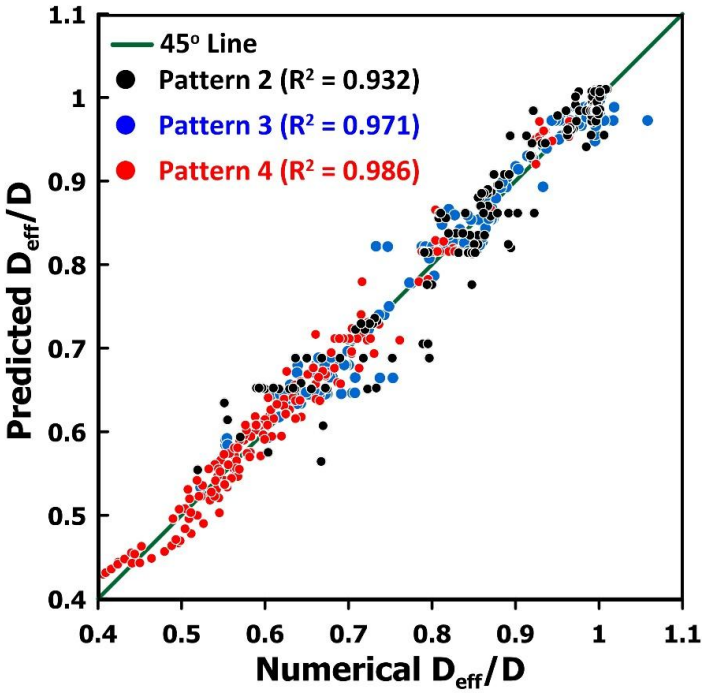

Figure 2.13. Parity plot of the prediction of the diffusion coefficient ratio D_{eff}/D for three different liquid coverage patterns and the FFNN of Figure 15.

2.4. Conclusions

This paper illustrates that the distribution of permeate on a membrane surface, which includes both the coverage of the surface area, and the pattern of species migration applied to the membrane, significantly influences the transport properties derived from permeation experiments. The effective diffusivity of the system varies with the fraction of the surface area of the membrane covered by the migrating species, the thickness of the membrane, and the geometry of the permeate applied to the membrane surface. For a flooded permeation cell, the intrinsic diffusivity is perfectly estimated. For membranes with partial liquid coverage, the effective diffusivity, as measured by the time-lag method, is lower than the intrinsic diffusivity of the membrane due to the multi-directional nature of the diffusion process. The experimental test methods used to evaluate PPE materials for protection against chemical warfare agents use partial liquid coverage. As a result, it may not be appropriate to use directly the transport properties obtained from these experimental methods to compare or generalize the protective performance of materials tested under different parameters such as material thickness, liquid coverage, and droplet pattern.

In instances where conducting experiments with flooded cells is either not feasible or impractical, applying a correction factor to the experimentally obtained transport properties can yield a more precise estimate of the intrinsic diffusivity. Subsequent experiments may be simulated using these intrinsic transport properties to investigate the impact of alterations in geometry and membrane thickness. Future research will involve conducting experiments to both assess and enhance the precision of our model, as well as to compare it against empirical data. Moreover, it would be interesting to investigate experimentally and numerically mixed-matrix or hybrid membranes to determine the estimation errors in their transport properties when characterized with the time-lag method. These newer membranes incorporate a reactive filler capable of neutralizing toxic chemicals as a means of detoxification[77–79].

Author Contributions: conceptualization, A.B. and J.T.; methodology, A.B., V.L. and J.T.; software, J.T.; validation, A.B. and J.T.; formal analysis, A.B. and J.T.; investigation, A.B., V.L. and J.T.; data curation, A.B. and J.T.; writing—original draft preparation, A.B. and J.T.; writing—review and editing, A.B., V.L. and J.T.; supervision, V.L. and J.T.; project administration, J.T.;

funding acquisition, J.T. All authors have read and agreed to the published version of the manuscript.

Funding: This research was funded by the Natural Science and Engineering Research Council (NSERC) Canada, Discovery Grant (DG), grant number RGPIN-2018-04433 (JT).

Data Availability Statement: Data are available upon request.

Conflicts of Interest: The authors declare no conflicts of interest. The funders had no role in the design of the study; in the collection, analyses, or interpretation of data; in the writing of the manuscript; or in the decision to publish the results.

Chapter 2: Appendix A

When you want to find an accurate model quickly that could be used for predicting a dependent variable, such as the diffusion coefficient ratio (D_{eff}/D), an artificial neural network can be easily used. Artificial neural networks are now commonly used for a large number of engineering applications, making use of the high degree of plasticity in their structure to encapsulate the underlying causal relationship between input and output data. In this investigation, a three-layer feedforward neural network (FFNN) was used to predict the diffusion coefficient ratio (D_{eff}/D) as a function of two input process variables. It is believed that a three-layer neural network is more than adequate to model the current problem. Cybenko[80] showed that a three-layer FFNN was sufficient to encapsulate any input–output relationship if a sufficient number of neurons were used. This appendix provides all the details to develop and use the final FFNN for the prediction of (D_{eff}/D).

The first step is to choose the set of independent variables that have a high probability of accurately inferring the dependent variable. In this case, two variables with the most impact, namely the thickness of the membrane and the liquid coverage fraction, were chosen to predict (D_{eff}/D) as the output of the FFNN. These choices fix the number of neurons in the input and output layers: three neurons in the input layer including the bias and one neuron in the output layer as shown in Figure 2.12. The number of neurons in the hidden layer is typically determined by trial and error to ensure a good prediction while avoiding overtraining. The selected neural network of Figure 2.12 has seven neurons in the hidden layer, including the bias neuron. The input and the output variables

were scaled in the range of [0,1] using the minimum and maximum of each variable as shown in Equations (2.15) and (2.16). Because the thickness (L) varied from 0.0001 to 0.02 m, the logarithmic function was scaled instead of the actual thickness. The coverage fraction (CF) did not need scaling because it already varies between zero and one, but the minimum and maximum were still retained in Equation (2.15) for completeness. For the output value, the minimum and maximum values were chosen as 0.35 and 1.15, respectively.

$$\begin{vmatrix} X_1 & X_2 \end{vmatrix} = \begin{vmatrix} \dfrac{\log_{10}(L)+4}{-1.7+4} & \dfrac{CF-0}{1-0} \end{vmatrix} \tag{2.15}$$

$$Y = \frac{\dfrac{D_{eff}}{D} - 0.35}{1.15 - 0.35} \tag{2.16}$$

The scaled inputs of the first layer are fanned out to all functional neurons in the hidden layer. Each functional neuron in the hidden layer simply transforms the weighted sum of the inputs of the first layer through a nonlinear function to calculate its output. In this investigation, a sigmoid function was used as the nonlinear function Equation (2.17). The weights between the neurons of the two adjacent layers are the parameters of the model. Each output H_j of the functional layer of the hidden layer is given by Equation (2.18).

$$f(\Psi) = \frac{1}{1 + e^{-\Psi}} \tag{2.17}$$

$$H_j = \frac{1}{1 + e^{-(W_{1j}X_1 + W_{2j}X_2 + W_{3j})}} = \frac{1}{1 + Exp\left(-\sum_{i=1}^{3} W_{ij} X_i\right)} \tag{2.18}$$

The outputs of the hidden layer, including the bias neuron of the hidden layer, are then sent to the output neuron. The output neuron performs the same task as the neurons of the second layer to generate the final output of the FFNN. A sigmoid function was also used as the transfer function of the output neuron. The output $\hat{Y}$ of the last layer is given by Equation (2.19).

$$\hat{Y} = \frac{1}{1 + e^{-(W'_{11}H_1 + W'_{21}H_2 + W'_{31}H_3 + W'_{41}H_4 + W'_{51}H_5 + W'_{61}H_6 + W'_{71})}} = \frac{1}{1 + Exp\left(-\sum_{j=1}^{7} W'_{j1} H_j\right)} \tag{2.19}$$

The fitting or training of a neural network boils down to minimizing the sum of squared errors between the actual values and predicted values by modifying the weights of the connections between the neurons of two adjacent layers. Typically, the data set is divided into three data subsets: training, validation, and testing. The neural model is initially fitted using the training data set whereas the validation data are used in parallel with the training data set to provide an unbiased evaluation of the model fit, a necessary step to avoid overtraining. The testing data set provides a further unbiased evaluation of the final model with data that the model has never seen. The FFNN structure of Figure 15 was chosen as the final model and can be represented mathematically in matrix form with Equations (2.20) and (2.21).

$$\begin{vmatrix} H_1 \\ H_2 \\ H_3 \\ H_4 \\ H_5 \\ H_6 \end{vmatrix} = \mathrm{f}\left(\overset{\mathrm{W_{ij}}}{\begin{vmatrix} 8.126 & 34.272 & -10.038 \\ -4.847 & 15.057 & -1.522 \\ -2.454 & 16.699 & -4.180 \\ -4.192 & -1.247 & 3.337 \\ 3.884 & 0.764 & -2.669 \\ -6.086 & 49.982 & -4.629 \end{vmatrix}} \bullet \begin{vmatrix} X_1 \\ X_2 \\ 1 \end{vmatrix} \right) \tag{2.20}$$

$$\hat{Y} = \mathrm{f}\left(\overset{\mathrm{W'_{jk}}}{\begin{vmatrix} 1.703 & 4.008 & -3.263 & -23.176 & -24.287 & -1.097 & 23.972 \end{vmatrix}} \bullet \begin{vmatrix} H_1 \\ H_2 \\ H_3 \\ H_4 \\ H_5 \\ H_6 \\ 1 \end{vmatrix} \right) \tag{2.21}$$

The only hyperparameter that was changed in the development of the neural network was the number of neurons in the hidden layer. The model could be simplified with a loss of accuracy in the predictions. The relative percentage prediction errors were 5.33% ± 5.04, 3.58% ± 3.18 and 2.44% ± 2.36 for three, five, and seven hidden neurons (including the bias), respectively. The maximum values of the relative percentage errors were 24.9%, 16.5%, and 15.4%, respectively.

Chapter 3 - Experimental Examination of the Permeation of Chemicals Through Common Protective Materials.

Alex Bicket[1], Vivian Lau[2] and Jules Thibault[1]

[1]Department of Chemical and Biological Engineering

University of Ottawa, Ottawa, Ontario, Canada K1N 6N5

Jules.Thibault@uottawa.ca

[2]Defence Research and Development Canada

Ralston, Alberta, Canada T1A 8K6

vivian.lau@drdc-rddc.gc.ca

Abstract

Previous work by the same authors used numerical methods to simulate the permeation of liquids through rubbery polymer membranes, identifying that certain testing methods would introduce errors in the estimated transport properties. In this study, a series of physical permeation experiments were performed to replicate the simulation results and provide experimental data for simulating identical experiments. This approach aims to compare and validate the synergy between simulations and experiments. Validation is crucial to ensure that numerical simulations accurately predict experimental results, minimizing the need for experiments with highly hazardous and toxic chemicals. The results presented show a promising correlation between experimental and simulation outcomes. Additionally, experimental data are necessary to determine the transport properties of polymeric membranes, enabling accurate simulations.

3.1 Background Information

Personal Protective Equipment (PPE) is essential for limiting exposure and reducing the risk of injury from chemical hazards. When personnel face potential exposure to hazardous chemicals, it is crucial to select appropriate PPE to ensure adequate protection. The equipment must be thoroughly characterized and tested to understand its protective capabilities, allowing for effective management of exposure and risk. To properly characterize PPE, rigorous physical testing is

conducted against various standards or challenges[56,57,65] to determine its effectiveness against specific threats. For liquid hazards that can permeate or damage the skin, PPE must prevent any contact with the skin. This often involves selecting materials that are both impermeable to the hazardous liquid and flexible, such as rubbery polymers, which are ideal for manufacturing gloves and boots where dexterity is vital. Some of the most hazardous classes of chemicals are Chemical Weapons (CW) or Chemical Warfare Agents (CWA), regulated by the Chemical Weapons Convention (CWC)[1]. Military personnel and first responders attending chemical incidents involving CW often face contamination risks, necessitating the design and testing of PPE to meet these challenges. One common test method is described in the US Army TOP 08-2-501A operational procedure[57], which involves permeation testing of materials with chemical agents or simulants. Known as swatch testing, this method uses three permeation cell configurations: convective flow, dual flow, and static diffusion. The procedure provides test parameters for liquid or vapor penetration swatch testing. For example, when testing nerve agents like GD (military designation of Soman) and VX (Venomous Agent X), it is recommended to apply ten 1-µL drops on the material swatch. If the aim is to determine the material's transport properties, using drops instead of full surface coverage can introduce significant errors in estimating these properties. These errors may lead to an optimistic assessment of PPE performance, which must be considered when interpreting test results.

To properly characterize a membrane–permeate system, it is essential to understand how the permeate moves through the membrane and the time it takes to break through. For rubbery polymer membranes, we use solution-diffusion theory, which applies to non-porous materials with non-crystalline structures. This theory accounts for the sorption at the liquid-membrane surface and the diffusion of permeate through the material based on the Brownian movement of molecules within the membrane matrix[62]. Physical permeation experiments allow us to estimate the transport properties of the permeant through the membrane using the time-lag method[60,81]. In a single time-lag experiment, it is possible to directly estimate the permeability (P) and diffusivity (D) of the membrane. While the solubility of the permeate in the membrane is typically determined using solubility experiments, it can also be estimated using the time-lag method. The relationship between permeability (P), solubility (S), and diffusivity (D) is described by Equation (3.1).

$$P = DS \tag{3.1}$$

The time-lag (θ) is determined when the steady-state permeation rate is achieved using the plot of the amount of permeate accumulated as a function of time. The value of θ is found at the intersection of the extrapolated line of constant slope from the permeate accumulation curve with the time axis when steady-state permeation is achieved. The membrane diffusivity is then estimated from the time lag and membrane thickness using Eq. (3.2). The membrane permeability is calculated from the constant rate of permeation and as a result, the membrane solubility can then be estimated using Eq. (3.1).

$$\theta = \frac{L^2}{6D} \tag{3.2}$$

Where L is the membrane thickness. Under steady state, we can use the permeation rate to calculate the membrane permeability using Eq. (3.3).

$$P = \frac{dm}{dt}\frac{L}{A\,\Delta C} \tag{3.3}$$

In Equation (3.3), *dm/dt* is the rate of change of the amount of permeant having diffused through the membrane into the sampling chamber measured by mass. This rate of change can be evaluated from the slope of the plot of the amount accumulated as a function of time. ΔC is the transmembrane mass concentration difference and A is the surface area of the membrane available for diffusion. With the estimated values of the permeability and diffusivity, the solubility can be calculated using Eq. (3.1). These intrinsic parameters of the membrane for a given permeant are required to assess the effectiveness the material against a given hazard.

In simpler systems where one-dimensional diffusion is dominant, we can calculate an analytical solution to the diffusion of the permeate through the membrane. These scenarios occur when the entire membrane surface is covered with a homogeneous layer of permeate, which diffuses downward at equal rates, creating a concentration profile across the membrane. In this case, Fick's first law of diffusion (Equation (3.4)) can be applied[64], where J_A is the flux of substance A permeating through the membrane, D_{AB} is the diffusivity of substance A in substance B (the membrane) and c_a is the concentration of A within the membrane. This equation applies at all

points within the membrane, and the flux varies as a function of time until steady-state permeation is achieved.

$$J_A = -D_{AB}\frac{dc_A}{dx} \tag{3.4}$$

At steady-state permeation, Equation (3.4) can be integrated to give Equation (3.5):

$$J_A = \frac{D_{AB}\,(c_{A1} - c_{A2})}{x_2 - x_1} \tag{3.5}$$

In this case, $x_1 = 0$ and $x_2 = L$, respectively for the feed and permeate sides of the membrane. The concentration of permeate applied to the membrane surface is known and it is assumed that the concentration on the permeate side of the membrane is zero. Then, the flux can be multiplied by the surface area of the membrane and the time to yield the total mass of permeate that has moved through the membrane, as given in equation (3.6).

$$m_A = \frac{D_{AB}(c_{A1} - c_{A2})At}{x_2 - x_1} \tag{3.6}$$

Equation (3.6) applies only to the steady-state portion of the permeation experiment. However, the time-lag method is a dynamic experiment, such that Equation (3.6) does not apply for the entire experiment, but only when a steady state is achieved. In that case, it will be necessary to use a graphical method, or a numerical method combined with a regression algorithm to simulate the entire experiment and determine the transport parameters of the membrane.

3.2 Materials, Apparatus, and Methods

3.2.1 Materials

Dimethyl methylphosphate (DMMP, >97%) and methyl salicylate (MeS, >99%) were purchased from Aldrich and used as received. LC-MS grade water was obtained from a Millipore Synergy water purification system. LC-MS grade methanol and acetonitrile were obtained from Honeywell Riedel-de Haen; LC-MS grade formic acid was obtained from Supelco. Glove material samples were cut from commercially available nitrile gloves (Kimtech Purple Nitrile Xtra Powder Free,

and Ansell Protective Products Sol-Vex), and military off-the-shelf butyl gloves (Airboss Defense NBC Gloves, NSN 8415219212172).

3.2.2 Membrane solubility experiments

Square samples of materials were cut from gloves (3 cm x 3 cm) and measured in several locations for thickness with an outside micrometer (Starrett). Each swatch was weighed dry and then placed in an 80 mL beaker and covered with 15 mL of solvent (50% methanol in water (v/v), DMMP or MeS). The swatches were removed at set time points, gently blotted dry with a lint-free tissue, weighed, and re-submerged in the solvent. Experiments were carried out at room temperature (24-27°C) in triplicates.

3.2.3 Membrane permeation experiments

Tests were performed using a static Franz diffusion cell (PermeGear Inc, part number 4G-02-00-25-20) with a 20 mL receptor volume and 25-mm diameter effective diffusion area (4.91 cm^2). A swatch of polymer material was sandwiched between the receptor compartment and the donor compartment. A magnetic stir bar was added to the receptor compartment, which was then filled with 50% methanol in water (v/v) as the receptor solution. This solvent mix was chosen because methanol does not degrade the nitrile or butyl rubber material samples and did not significantly swell the material in solubility testing. The apparatus was stirred for 30 minutes to equilibrate the polymer material, and then 600 µL of DMMP was added to the donor compartment to fully cover the material surface. A glass slide was used to cover the donor compartment to prevent evaporation. At pre-determined time points, 500 µL of the receptor solution was taken from the side arm for LC-MS/MS analysis, and an equal volume of fresh receptor solution was added to the receptor compartment. The samples were diluted as needed with 50% methanol in water (v/v) prior to the analysis. Experiments were carried out at room temperature (24-27°C) and carried out in duplicates. Figure 3.1 and Figure 3.2 show the experimental apparatus used to conduct permeation experiments based on a Franz diffusion cell.

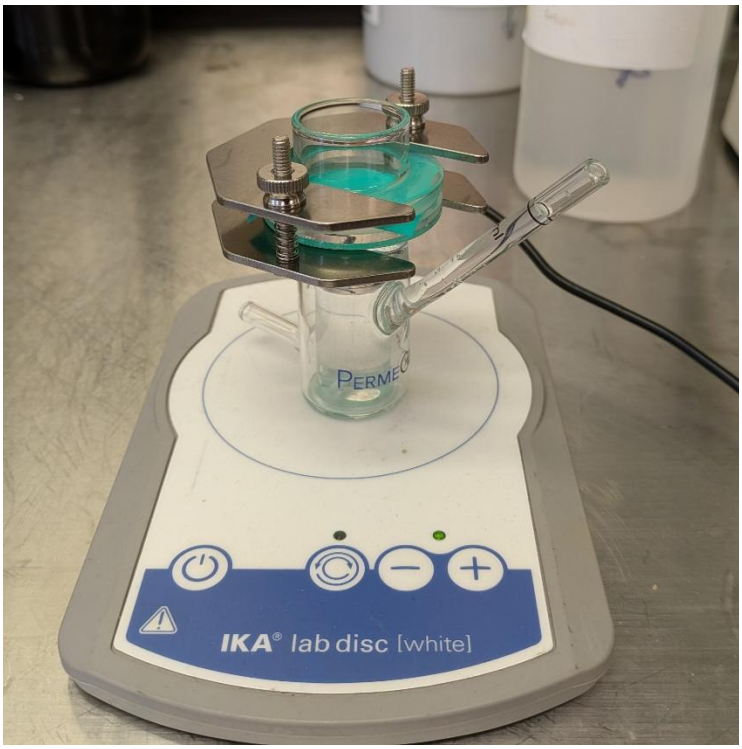

Figure 3.1: A Franz diffusion cell used in the membrane diffusion experiments with a circular sample of green nitrile clamped between the donor and receptor chambers. Photo by Dr Vivian Lau.

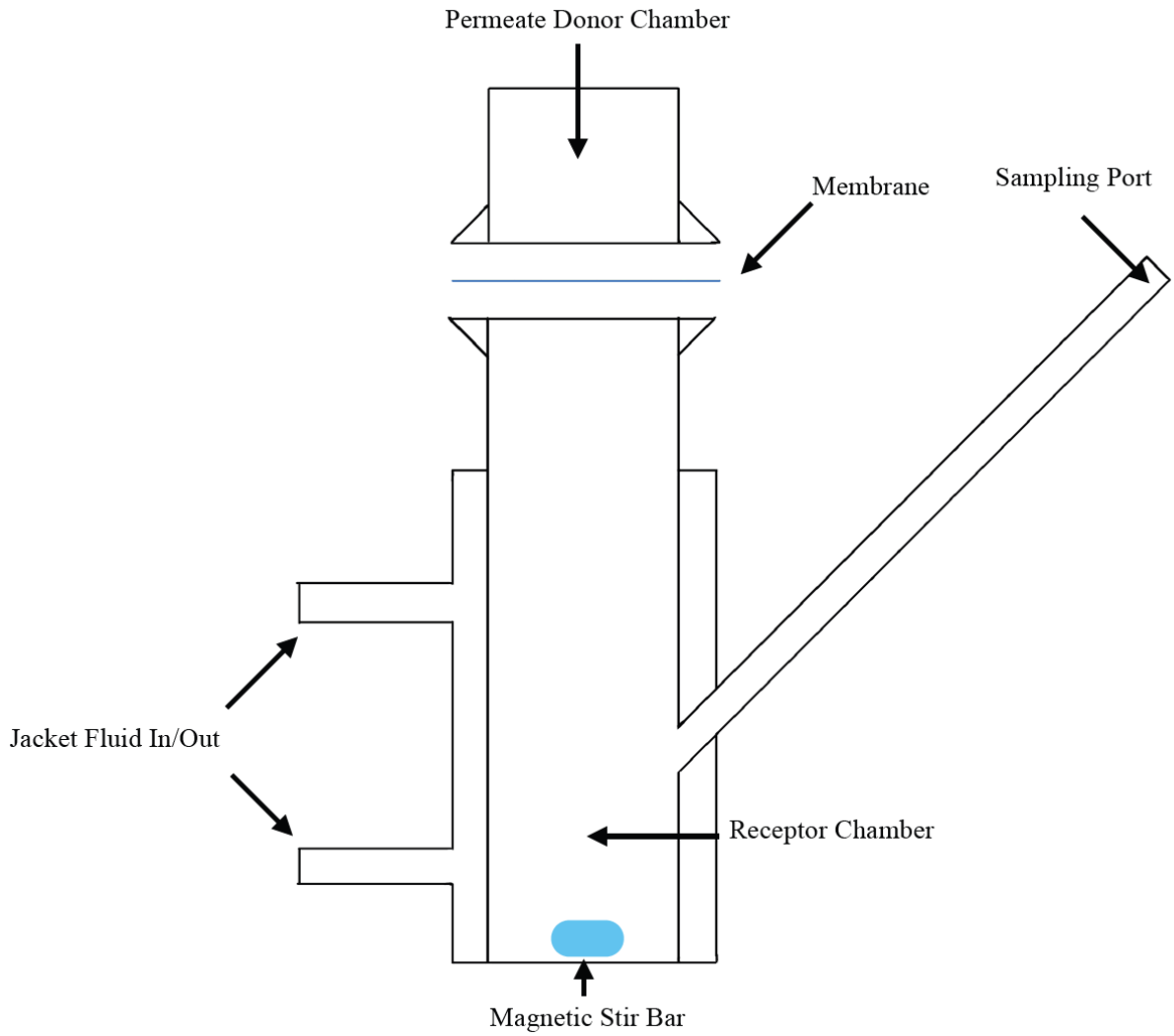

Figure 3.2: Diagram of a Franz Diffusion Cell. Drawn by Alex Bicket.

3.2.4 LC-MS/MS analysis

Quantitative analysis of permeation over time was carried out with a Waters Acquity I-Class UPLC coupled to a Xevo TQ-XS triple quadrupole mass spectrometer using an electrospray ionization source (ESI) operating in positive mode with Argon as the collision gas. Chromatography was carried out with an Acquity UPLC BEH C18 column (2.1 x 50 mm, 1.7 µm) maintained at 35°C, with 0.1% formic acid in water as the aqueous component and 0.1% formic acid in acetonitrile as the organic component in the mobile phase. DMMP was analyzed in multiple reaction monitoring

mode, using 125.0 → 111.0 (m/z) as the quantifier transition and 125.0→ 93.0 (m/z) as the qualifier transition. The samples were quantified against a calibration curve prepared in 50% methanol in water (v/v) and was linear from 3 pg/mL to 300 ng/mL.

All experiments were conducted at Defence Research and Development Canada (DRDC) Suffield Research Center by trained personnel and in accordance with recognized safety procedures and regulations concerning the use and safe handling of hazardous chemicals.

3.2.5 Mathematical Methods

After obtaining data from the experimental methods described above, the following mathematical methods were used to determine the transport properties of the experimental systems. Three separate methods were applied to the experimental data for comparison against each other and the experimental data itself.

3.2.5.1 Method 1 – Using the slope and time-intercept of the dynamic accumulation curve.

Using the method described in the section titled "Membrane permeation experiments" to generate permeation data, when the permeate accumulation is plotted against time, the resulting curve becomes locally linear as it reaches steady state. The slope of this linear portion can be extrapolated to the time axis, providing the value of the time lag (θ), which is then used to calculate the diffusion coefficient (*D*) using Eq. (2). The permeation rate in the steady-state portion of the curve allows us to calculate the permeability (*P*) using Equation (3.3). With the known diffusivity and permeability, we can calculate the solubility by applying Equation (3.1).

3.2.5.2 Method 2 – Using a nonlinear fit to estimate *D* and *S*

Fick's second law of diffusion, analytically solved by the separation of variables, can be used to determine the concentration of permeate throughout the membrane as a function of time (Equation (3.7)).

$$c(z,t) = c_0\left(1-\frac{z}{L}\right) - 2\frac{c_0}{\pi}\sum_{n=1}^{\infty}\frac{1}{n}\sin\left(\frac{n\pi z}{L}\right)\exp\left(-\frac{Dn^2\pi^2 t}{L^2}\right) \tag{3.7}$$

In this equation, c_0 is the upstream or bulk liquid concentration of liquid on the feed side of the membrane after the step change in concentration (in this case, the application of the liquid permeate to the membrane) is applied. Combining Fick's first law of diffusion with Equation (3.7) leads to the determination of the flux at any position within the membrane (Equation (3.8)).

$$J(z,t) = -D\frac{dc(z,t)}{dz} = \frac{C_0 DS}{L} + 2\frac{C_0 DS}{L}\sum_{n=1}^{\infty}\cos\left(\frac{n\pi z}{L}\right)\exp\left(-\frac{Dn^2\pi^2 t}{L^2}\right) \quad (3.8)$$

When $x=L$, at the boundary of the membrane and the receptor fluid, Eq. (3.8) takes the following form (Equation (3.9)).

$$J(L,t) = \frac{C_0 DS}{L} + 2\frac{C_0 DS}{L}\sum_{n=1}^{\infty}(-1)^n \exp\left(-\frac{Dn^2\pi^2 t}{L^2}\right) \quad (3.9)$$

Integrating the flux equation with respect to time allows us to calculate the total mass of permeant ($m(t)$) that has moved through the membrane into the receptor volume at any time t (Equation (3.10)).

$$m(t) = \int_0^t J(L,t)\,A\,dt \quad (3.10)$$

Using Equations (3.9) and (3.10), we can determine $m(t)$ for any values of D and S. By applying nonlinear regression analysis, we can identify the values of D and S that best fit the experimental accumulation curves, The nonlinear least squares method described by Marquardt[82] was used, minimizing the objective function F in Equation (3.11).

$$F = \underset{D,S}{Min}\sum_{i=1}^{N}\left(m_i(t)_{\text{Predicted}} - m_i(t)_{\text{Experimental}}\right)^2 \quad (3.11)$$

With D and S determined, we can use Equation (3.1) to calculate P.

3.2.5.3 Method 3 – Nonlinear fit to estimate D with known S.

The final method uses the results of the solubility experiments described in the section "Solubility Testing" to provide a known, experimentally determined value of S. The same least squares

regression from Method 2 is then applied to determine *D*, minimizing the objective function described in Equation (3.11). However, in the case, only finding the optimal values of *D* to achieve the best fit, rather than both *D* and *S*.

3.3 Results and Discussion

3.3.1 Solubility Testing

Solubility testing was done with both the permeate and the solvent to determine the solubility of those chemicals in the glove material. The results are presented in Table 3.1.

Table 3.1. Results of the solubility tests.

Material	Solute	Solubility (g solvent/g material)	Experiment Time (s)
Nitrile Rubber	Water-Methanol (9:1)	0.0750	1320
Butyl Rubber	Water-Methanol (9:1)	0.0064	1418
Nitrile Rubber	Methyl Salicylate	3.0165	1440
Butyl Rubber	Methyl Salicylate	0.1277	1440
Nitrile Rubber	DMMP	1.1881	1360
Butyl Rubber	DMMP	0.0048	1360

As expected, the butyl rubber glove material absorbed significantly less liquid than the nitrile rubber material. Previous work by various authors has shown that butyl rubber is more effective as a protective material against chemical warfare agents, which is reflected in its much lower solubility for simulants[25,65,83,84]. During experiments, the nitrile material exhibited much more significant swelling and mass gain from the solute within the material. In all three cases examined, the liquid uptake into nitrile rubber was at least an order of magnitude greater than that into butyl rubber. Additionally, the uptake of the chosen solvent in the receptor chamber of the experimental apparatus (water-methanol solution) was significantly lower in both rubber materials compared to the uptake of the test permeates (Methyl Salicylate and DMMP). This large difference in affinities

between the liquids confirms that there will be minimal impact on permeation testing from the membrane absorbing the chosen solvent from the receptor chamber.

3.3.2 Permeation Testing

Permeation testing was conducted using the methods described above. The resulting experimental data were used to generate permeation curves, and the time-lag method was applied to determine the membrane's transport properties. The three methods described above were used to calculate the transport properties of the systems tested and are compared below. Runs 1–3 were conducted with Ansell green nitrile gloves, Runs 4–7 with Kimtech purple nitrile gloves, and Runs 8–9 with Airboss butyl rubber gloves, as described in the materials section. Runs 6 and 7 were conducted with 20% of the membrane surface area covered with drops of permeate, while the remainder of the experiments had complete coverage. Other physical properties are given in Table 3.2.

Table 3.2. Physical properties of experimental systems for each run.

Run	1	2	3	4	5	6	7	**8**	**9**
Chemical	DMMP	DMMP	DMMP	DMMP	DMMP	DMMP	DMMP	DMMP	DMMP
Material	Nitrile Rubber	Nitrile Rubber	Nitrile Rubber	Nitrile Rubber	Nitrile Rubber	Nitrile Rubber	Nitrile Rubber	Butyl Rubber	Butyl Rubber
Coverage	1.000E+00	1.000E+00	1.000E+00	1.000E+00	1.000E+00	2.000E-01	2.000E-01	1.000E+00	1.000E+00
L (m)	2.600E-04	2.600E-04	2.600E-04	1.200E-04	1.200E-04	2.600E-04	2.600E-04	1.700E-04	1.700E-04
D (m^2/s)	2.270E-12	3.061E-12	2.774E-12	1.387E-12	6.097E-12	1.547E-12	2.172E-12	2.666E-13	2.333E-13
d (m)	2.500E-02	2.500E-02	2.500E-02	2.500E-02	2.500E-02	2.500E-02	2.500E-02	2.500E-02	2.500E-02
Rho (kg/m^3)	1.145E+03	1.145E+03	1.145E+03	1.145E+03	1.145E+03	1.145E+03	1.145E+03	1.145E+03	1.145E+03
P (m^2/s)	1.149E-12	3.602E-12	3.214E-12	3.139E-12	2.288E-12	1.169E-12	5.341E-13	2.367E-17	4.956E-17
S (g/g)	5.020E-01	1.177E+00	1.159E+00	2.264E+00	3.753E-01	7.556E-01	2.459E-01	8.879E-05	2.124E-04

For each permeation experiment, the dynamic permeation data were used to estimate *P*, *D*, and *S* by applying the three mathematical methods discussed above. The values of these transport coefficients are given in Table 3.2 for the nine permeation experiments. For Method 1, *D* and *P* were determined from the plot of the accumulated amount of the permeating species as a function of time, using the time lag value and the steady-state slope, respectively. *S* was then determined from the ratio of *P* and *D* (Eq. (1)). For Method 2, *D* and *S* were determined by regression analysis, which allows us to estimate *P*. For Method 3, the experimental value of *S*, obtained from the solubility tests, was used such that only *D* needed to be determined with the regression analysis; *P*

was determined from the product of *D* and *S*. The estimated transport parameters with each of the methods are presented in Table 3.3. In addition, the experimental data of the nine runs are plotted in Figure 3.3 through Figure 3.11. On the same figures, the steady-state line, extrapolated to the time axis to determine the time lag for each run, is shown in addition to the fitted curve for Methods 1 and 2. Typically, a permeation experiment should be conducted for a period corresponding to three times the time lag. In most experiments, the permeation time was shorter, which may have affected the accurate evaluation of the transport properties. Despite the relatively good fit of the experimental data with the three methods, the variation of the transport parameters is relatively large. It would be important to improve the accuracy and duration of these experiments to increase trust in the data obtained.

Table 3.3. Results of each run of experiments when mathematical Methods 1-3 were applied.

Run	Method 1			Method 2				Method 3			
	D (m^2/s)	S* (g/g)	P (m^2/s)	D (m^2/s)	S (g/g)	P* (m^2/s)	SQR	D (m^2/s)	S^+ (g/g)	P (m^2/s)	SQR
1	2.270E-12	5.020E-01	1.149E-12	1.305E-12	2.825E+00	3.687E-12	6.000E+00	1.923E-12	1.188E+00	2.285E-12	1.677E+01
2	3.061E-12	1.177E+00	3.602E-12	2.094E-12	2.217E+00	4.642E-12	2.677E+01	2.968E-12	1.188E+00	3.526E-12	5.907E+01
3	2.774E-12	1.159E+00	3.214E-12	1.995E-12	2.014E+00	4.018E-12	3.502E+01	2.653E-12	1.188E+00	3.152E-12	5.102E+01
4	1.387E-12	2.264E+00	3.139E-12	5.024E-12	4.330E-01	2.175E-12	5.279E+02	2.035E-12	1.188E+00	2.417E-12	6.405E+02
5	6.097E-12	3.753E-01	2.288E-12	8.884E-12	2.443E-01	2.170E-12	1.145E+02	2.083E-12	1.188E+00	2.474E-12	3.585E+02
6	1.547E-12	7.556E-01	1.169E-12	6.068E-13	6.934E+00	4.208E-12	1.718E+00	1.152E-12	1.188E+00	1.368E-12	1.678E+01
7	2.172E-12	2.459E-01	5.341E-13	2.101E-12	2.159E-01	4.537E-13	3.151E+00	9.191E-13	1.188E+00	1.092E-12	1.083E+01
8	2.666E-13	8.879E-05	2.367E-17	6.933E-14	7.216E-03	5.003E-16	5.134E-09	7.481E-14	4.801E-03	3.592E-16	6.026E-09
9	2.333E-13	2.124E-04	4.956E-17	4.213E-14	2.620E-01	1.104E-14	7.202E-09	7.760E-14	4.801E-03	3.725E-16	2.643E-08

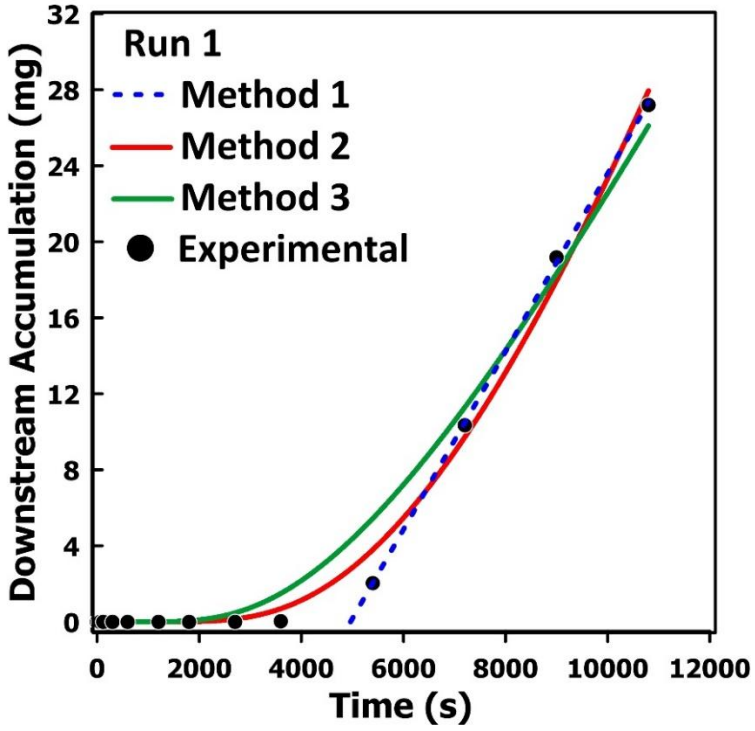

Figure 3.3: Downstream accumulation (mg) vs time (s) for Run 1.

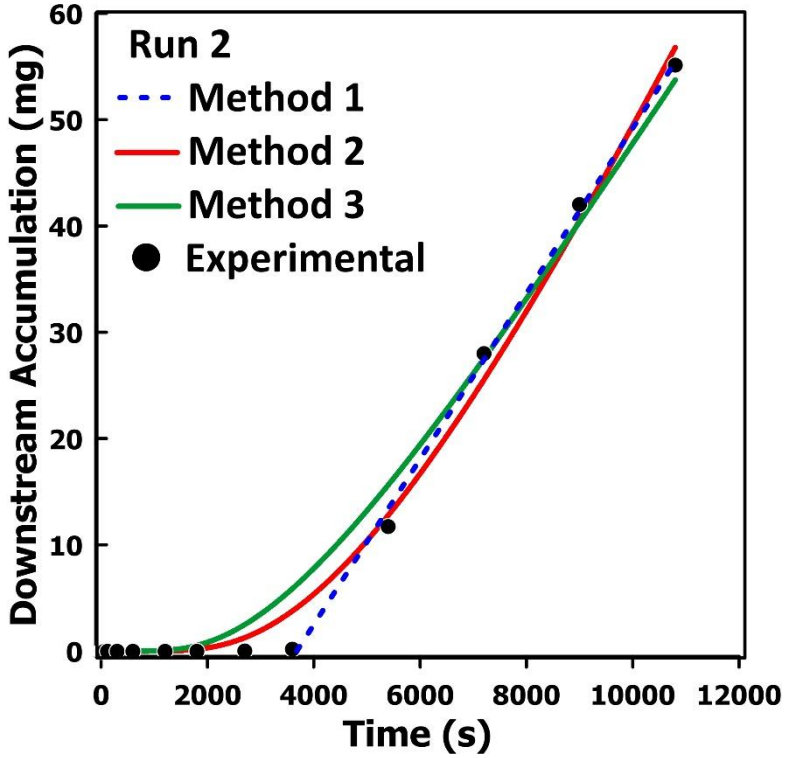

Figure 3.4: Downstream accumulation (mg) vs time (s) for Run 2.

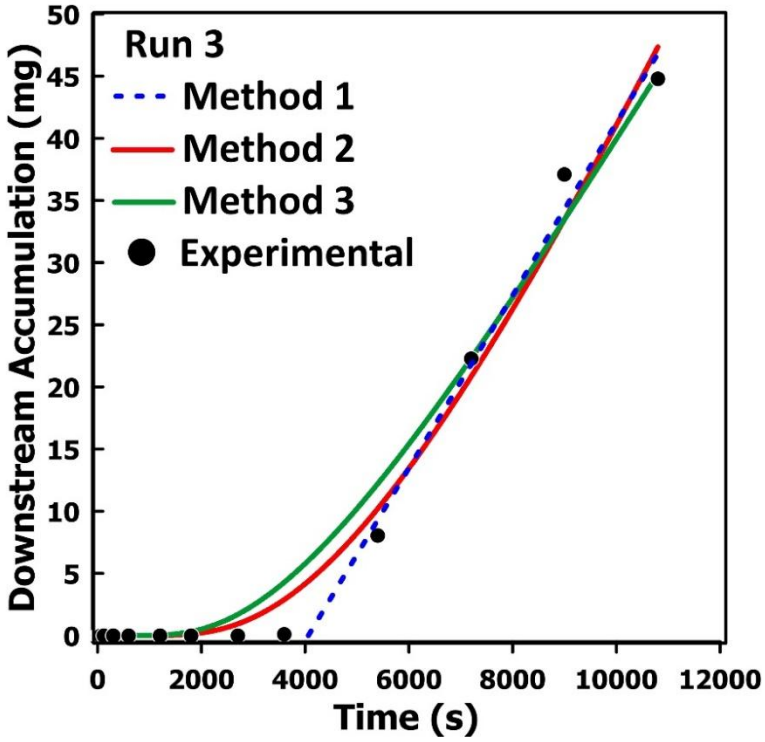

Figure 3.5: Downstream accumulation (mg) vs time (s) for Run 3.

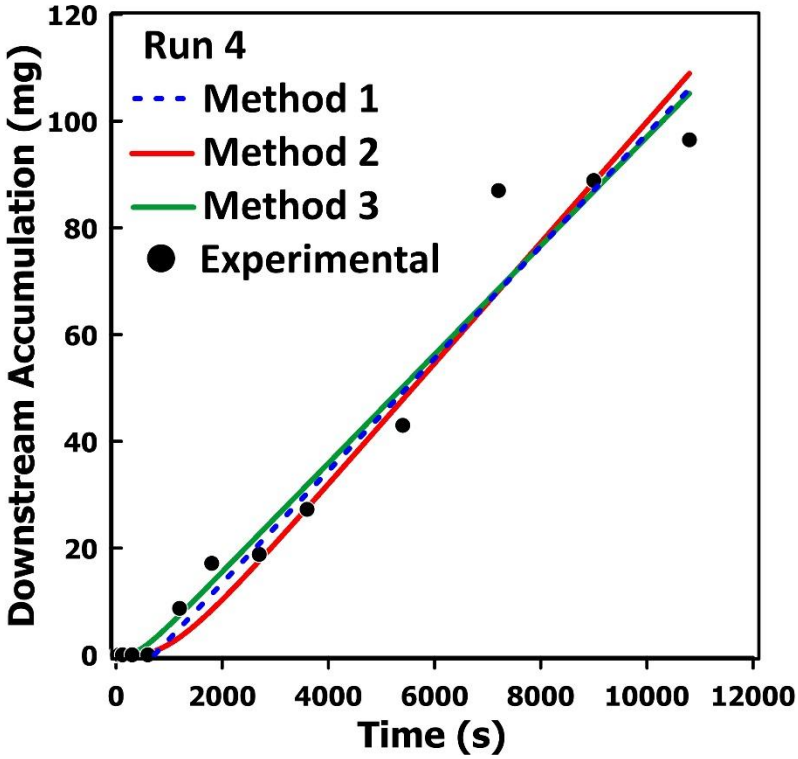

Figure 3.6: Downstream accumulation (mg) vs time (s) for Run 4.

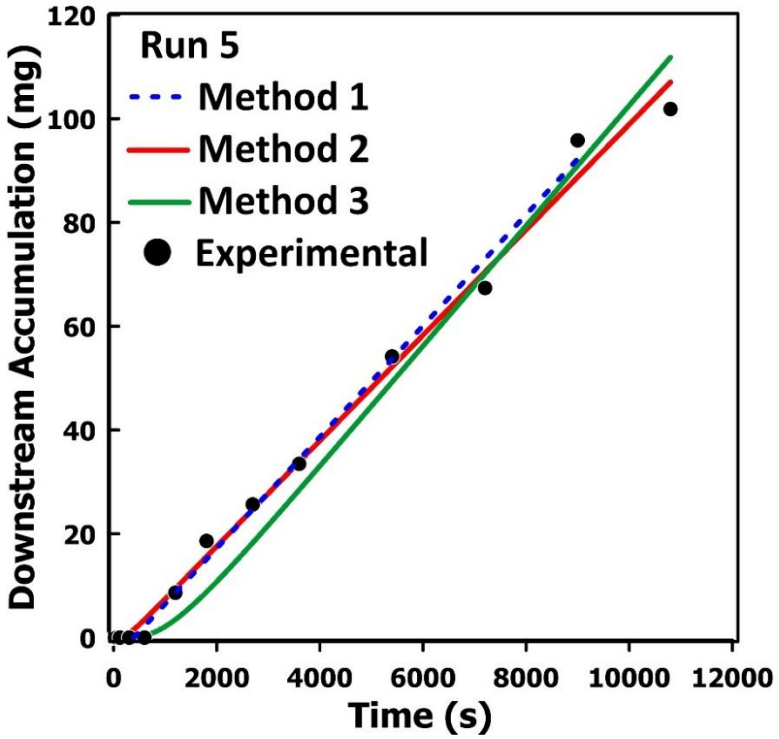

Figure 3.7: Downstream accumulation (mg) vs. time (s) for Run 5.

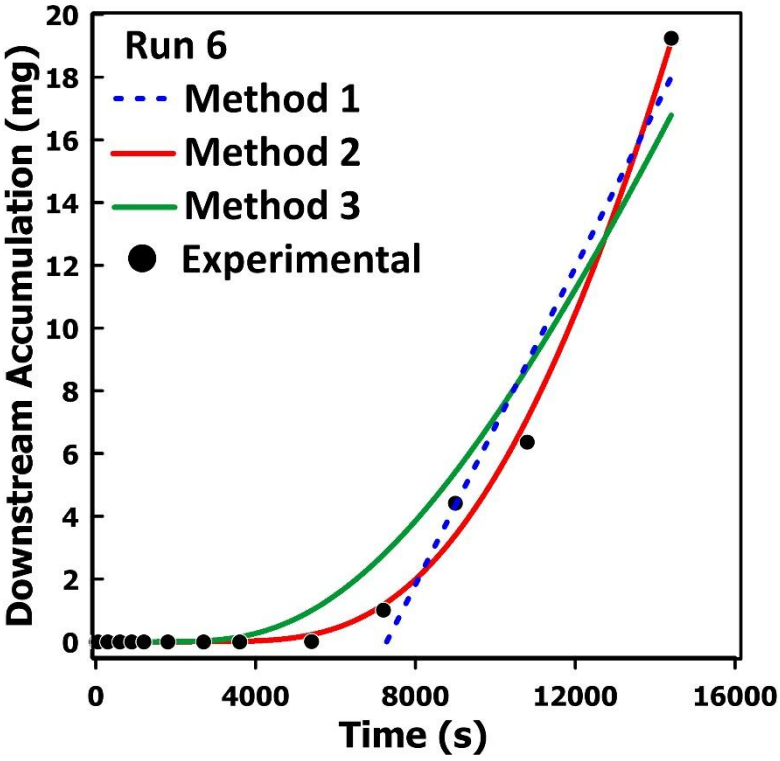

Figure 3.8: Downstream accumulation (mg) vs time (s) for Run 6.

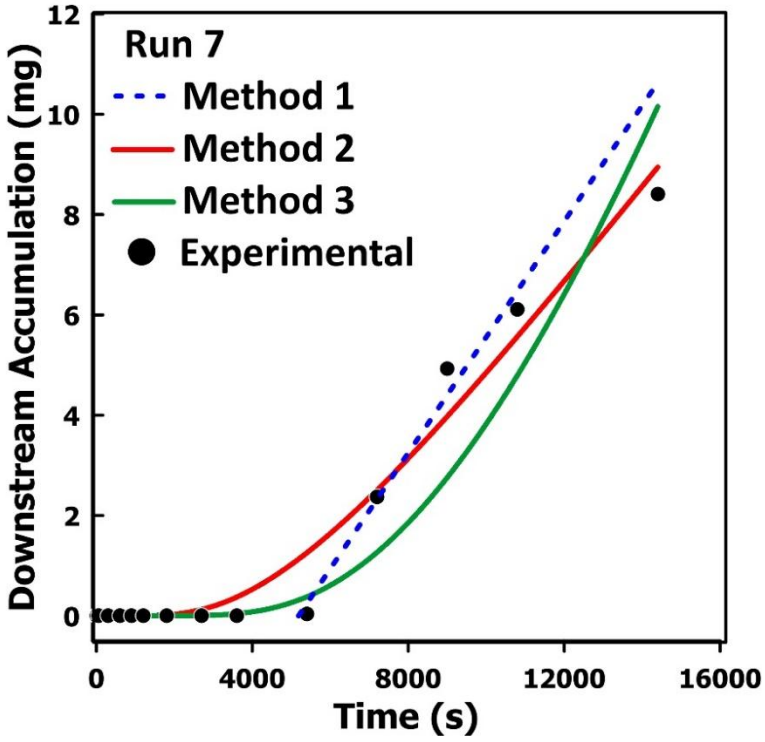

Figure 3.9: Downstream accumulation (mg) vs. time (s) for Run 7.

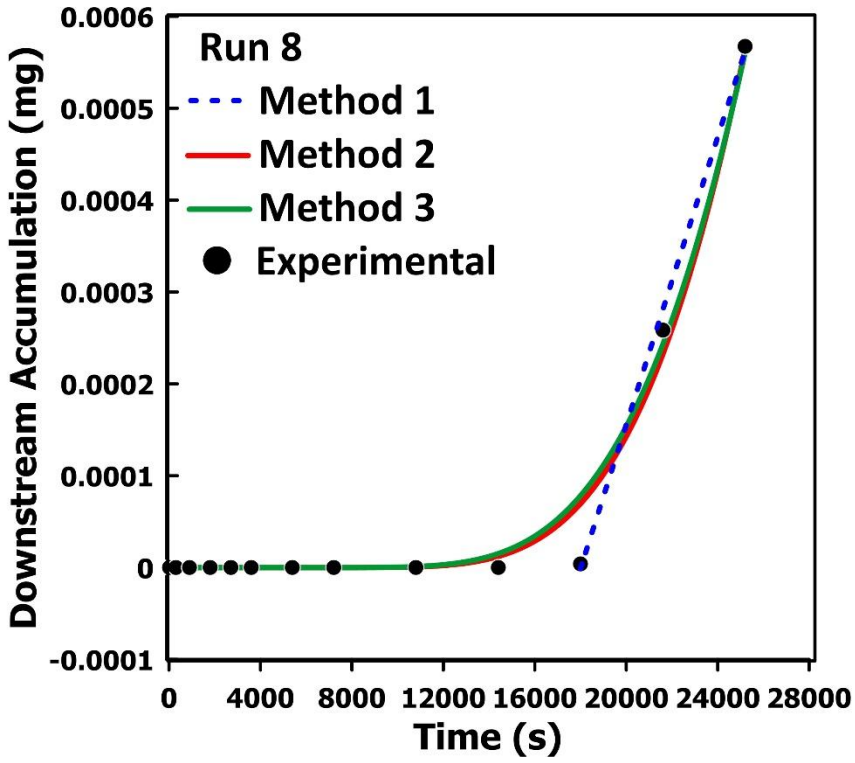

Figure 3.10: Downstream accumulation (mg) vs time (s) for Run 8.

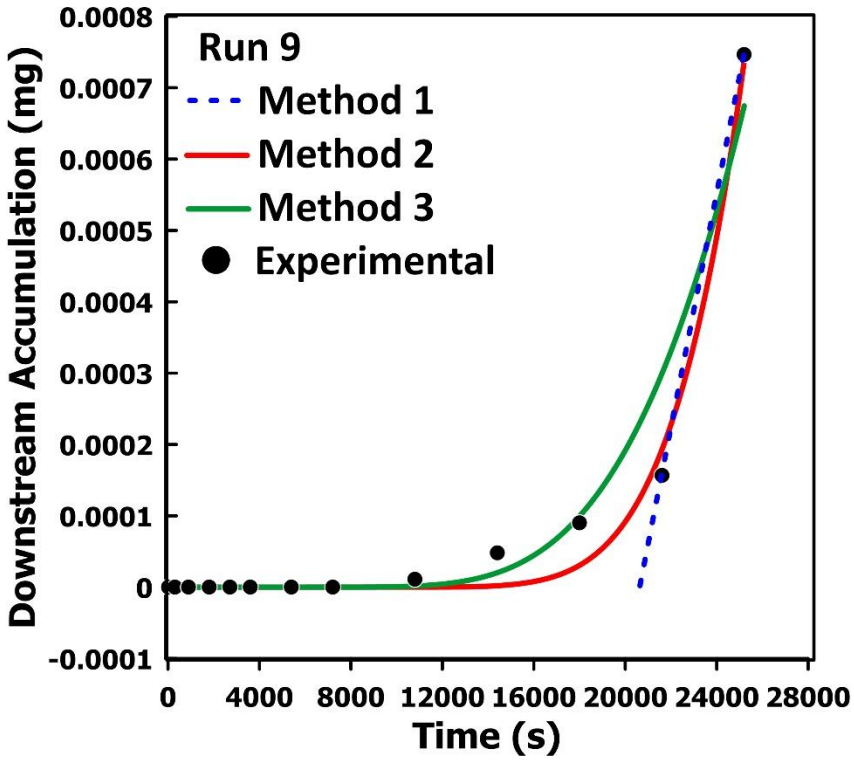

Figure 3.11: Downstream accumulation (mg) vs time (s) for Run 9.

Table 3.4 presents the averages and standard deviations of the transport properties presented in Table 3.3, as calculated with the three methods, grouped by experimental conditions including material-permeate system and the coverage fractions described in Table 3.2. Table 3.4 shows that the standard deviations for the estimation of *D* for Runs 1 to 5 (nitrile rubber, full coverage) are 57%, 82%, and 20% for Methods 1, 2, and 3, respectively. The standard deviations for Runs 6 and 7 (nitrile rubber, 20% coverage), are 34%, 78%, and 16%, respectively, whereas for Runs 8 and 9 (butyl rubber, full coverage) they are 10%, 35%, and 26%, respectively. In general, the variation in the estimation of *D* is lower with Method 3, where the solubility was determined via solubility tests and used as a constant in the regression analysis.

Results of Runs 1 to 5 and Runs 6 and 7 allow us to study the effect of the different liquid patterns on the estimation of the transport properties. Using the experimental results and the model derived in Chapter 2, it is estimated that *D* evaluated using the drop pattern should be approximately 78% of *D* evaluated with full liquid coverage. Experimental results show that *D* with the drop pattern is 59%, 35%, and 44% of the value of *D* with full coverage via Methods 1, 2, and 3. These results point out once more that the accuracy of the experiments must be drastically increased to estimate

transport properties more accurately. It can nevertheless be concluded that using a drop pattern on the upstream surface of the membrane leads to smaller D values, which need to be corrected to estimate the system's intrinsic *D*.

Experiments were conducted with different brands, thicknesses, and colors of nitrile gloves. When comparing the two brands/thicknesses of nitrile gloves, no significant differences in transport properties were observed. The results of the butyl rubber experiments are largely similar and generated a lower diffusivity value than the nitrile, which is to be expected based on the differences in material and previous works showing that butyl rubber is a more effective barrier material than nitrile for these types of chemicals[58,85].

Table 3.4. Average and Standard Deviation across the three different methods.

Run	Method 1			Method 2			Method 3		
	D (m^2/s)	S* (g/g)	P (m^2/s)	D (m^2/s)	S (g/g)	P* (m^2/s)	D (m^2/s)	S^+ (g/g)	P (m^2/s)
Average (1-5)	3.118E-12	1.095E+00	2.678E-12	3.860E-12	1.547E+00	3.338E-12	2.332E-12	1.188E+00	2.771E-12
St Dev (1-5)	1.783E-12	7.495E-01	9.802E-13	3.151E-12	1.144E+00	1.118E-12	4.542E-13	0.000E+00	5.396E-13
Average (6-7)	1.860E-12	5.008E-01	8.517E-13	1.354E-12	3.575E+00	2.331E-12	1.035E-12	1.188E+00	1.230E-12
St Dev (6-7)	4.415E-13	3.604E-01	4.491E-13	1.057E-12	4.751E+00	2.654E-12	1.644E-13	0.000E+00	1.953E-13
Average (8-9)	2.500E-13	1.506E-04	3.662E-17	5.573E-14	1.346E-01	5.770E-15	7.620E-14	4.801E-03	3.659E-16
St Dev (8-9)	2.355E-14	8.740E-05	1.830E-17	1.924E-14	1.802E-01	7.452E-15	1.968E-15	0.000E+00	9.450E-18

3.4 Conclusion

This paper has presented the results of a series of permeation experiments conducted to evaluate the transport properties of materials exposed to hazardous chemicals. In this investigation, samples of nitrile rubber and butyl rubber PPE were used. These experiments are paramount to determine the maximum time PPE can be used by first responders and military personnel to ensure adequate protection. Given the nature of the experiments, the number of data points collected, and the duration of the experiments are relatively low, which limits the accuracy to be expected from these experiments. It would be important to find ways to improve the latter two limitations to estimate more precisely and accurately the transport properties of PPE materials.

Three methods were used to estimate the material transport properties from the experimental data. Method 1 uses the time-lag method, whereas Methods 2 and 3 resort to a nonlinear regression

analysis. Method 1 is undoubtedly the easiest and most commonly used method to analyze the experimental data. However, in this investigation, it only relied on a few experimental data points to determine both the time lag and the steady-state slope of the plot of the accumulated amount of permeant as a function of time. All methods provided an estimate, albeit with large standard deviations, of the transport properties. The transport parameters can then be used to simulate different scenarios to gain a better understanding of the permeation of a toxic substance through PPE.

Results have shown clearly that the drop pattern of the toxic chemical on the upstream surface of the membrane has a major effect on the estimation of the membrane's transport properties. The experimental data for the drop pattern (20% coverage) had a higher variability than for a membrane with full coverage. Nevertheless, it is possible to correct the estimated transport properties based on the model derived in Chapter 2.

Future work should expand on further examine the impact of experimental conditions on the membrane's transport properties. It would also be highly desirable to find ways to improve the acquisition of the data in terms of quantity and duration of experiments. Unfortunately, infrastructure issues at DRDC Suffield caused significant experimental delays which truncated the scope of experiments able to be conducted. With the limited data available, the results for low fractional coverage of the surface area suggest further experiments are worth conducting. Future experiments should be conducted to provide more data points for comparison as well as examining the effects of multiple different thicknesses of membrane, different droplet patterns and confirming the magnitude of the error is system independent by analysis data using different permeates. Time limitations where some of the materials take a significant amount of time to breakthrough also posed issues and if possible future experiments should look to test longer time scales to generate full breakthrough curves, providing more data points for both the steady-state portion of the curve and the curve fitting overall.

Chapter 4 - Conclusions and recommendations

In this work, we have shown that experimental design can have a significant impact on calculated transport properties through numerical simulation of different experiments.

In the second chapter, the results of these simulations were examined to determine that the amount of surface area of a membrane covered affects the diffusion of permeate through that membrane. Where full coverage of the membrane is achieved, diffusion only occurs orthogonal to the surface of the membrane. However, when the surface of the membrane is not completely covered by the permeate, the diffusion occurs in three dimensions within the membrane due to concentration profiles not being uniform in the *z*-direction. This causes error in measurements as the membrane is not allowed to reach steady state before breakthrough occurs, leading to underestimation of D_{eff}. This effect is influenced by the pattern of permeate applied to the membrane, due to the interaction between the discrete concentration profiles within the membrane, further complicating diffusion, and the thickness of the membrane. Thinner membranes have little volume to saturate for incomplete coverage, which minimizes error, but interestingly, as the thickness increases, the error begins to go back down, specifically in the case of a finite sample of membrane with impermeability boundary conditions at the edges. This is likely due to the thickness of the membrane allowing diffusion to once again approach one-dimensional diffusion as the concentration profile within the membrane evens out and becomes uniform again. Unfortunately, the thicknesses of membranes that most amplify the error in diffusion are within the orders of magnitude of those of commonly used protective equipment items such as gloves. In this work, we were also able to demonstrate that the error in the experiment is independent of the experimental system itself – the value of D provided to the simulation did not impact the error when comparing D to the D_{eff} calculated from the simulation results. This suggests that the error is entirely related to the way permeate diffuses into and accumulates within the membrane, and is not dependant on the rate at which diffusion occurs, the temperature or the combination of membrane and permeate chosen, with the caveat that all of the cases tested were tested using solution diffusion theory which is valid for non porous rubbery polymer membranes and does not cover the case where pore flow constitutes a significant element of diffusion through a membrane. The largest single source of error in these experiments was determined to be the thickness of the

membrane, with maximum error values predicted at around 6 mm of thickness. Thickness in the mm order of magnitude is not uncommon in some protective equipment.

The third chapter analyzed data collected from physical experiments with the intention of replicating the simulation results. Infrastructure and availability issues with the experimental partner, DRDC Suffield, limited the scope of physical experiments, however the data that was analyzed showed promising results in support of the simulation work conducted in chapter 2. In testing done the variation of surface area coverage on the membrane did lead to variation in the calculated transport properties of the system with an optimistic prediction being rendered by lower coverage amounts. This is consistent with the results of the simulation experiments, however the experiments conducted had some limitations around the time length of the experiments and the limited number of experiments conducted limited the number of variables that could be tested. In this chapter we also compared three methods of calculating transport properties from plotted data, comparing the time lag method, and two non-linear regression methods. All produced acceptable results however the non-linear regression method which used experimental validation of the solubility proved more accurate that that which varied two variables. The regression methods offered the advantage over the time lag method that they can use non-steady state data in their curve fitting to contribute to predicting the diffusivity.

The conclusions of the two articles show that commonly used test patterns for challenging PPE against CWA cause error in the values of transport properties calculated and could lead to overestimation of breakthrough time, this error is maximized at thicknesses common in certain protective equipment widely relied upon. While the experimental design is chosen to simulate other desired outcomes better, without conducting experiments using flooded cell conditions or applying a correction factor the resulting transport properties should be used with care and the limitations of the experiments should be well understood. Experiments conducted to predict breakthrough times will provide accurate results only for conditions closely matching the experimental results (such as the geometry of contamination). The further actual contamination deviates from the experimental conditions the more an actual breakthrough would deviate from experimental breakthrough, particularly when the thickness of the membrane is in the magnitude band of highest levels of error. This also leads to the conclusion that transport properties calculated from these experiments are not accurate unless thin membrane samples are used and therefore

should be corrected. However, the calculation of a correction factor is straightforward with multiple possible methods:

1. Physical experiments with the same physical contamination pattern and thickness of membrane could be conducted and compared to flooded cell experiments to determine a correction factor.
2. Flooded cell experiments could generate accurate properties that could be used to simulate partial coverage and predict a correction factor. This, and option 1, are simplified by the irrelevance of the system chosen, correction factors could be determined with safer and cheaper components and applied to any experiments with the same physical parameters.
3. Use a FFNN, such as the one proposed in the second chapter, to provide a correction factor to the transport properties.
4. Use the experimental results to simulate the experiments and iterate on the value of transport properties provided to the simulation until the experimental results were reproduced.

Applying a correction factor to experimental transport properties determined using incomplete coverage experiments would allow for the use of the derived properties to accurately simulate other scenarios and expand the ability of researchers to conduct experiments safely and produce accurate simulation results. More accurate experimental results will lead to better evaluation of PPE effectiveness and allows anyone requiring that PPE to make better informed decisions about PPE selection and how to manage exposure should the PPE be contaminated to prevent injury.

Future work in this vein should expand upon the experiments analyzed in the third chapter to include increasing the run time to generate more full curves, running more experiments to confirm the impact of membrane thickness and patterns on the experiment and using that data to predict correction factors for commonly used experimental designs. As the test procedure described in US Army TOP 08-2-501A[57] is commonly used to evaluate protective equipment against CWA exposure, having accessible correction factors in literature should be a valuable tool for scientists conducting PPE testing or anyone evaluating results of these experiments. The simulation and experimental work could be easily done with common material thicknesses in most PPE and

should be relatively straightforward to conduct flooded cell experiments and simulate to calculate a correction factor to be applied.

References

(1) OPCW. Chemical Weapons Convention, 2020. https://www.opcw.org/chemical-weapons-convention.

(2) National Center for Biotechnology Information. *PubChem Compound Summary for CID 10461, Mustard gas.* https://pubchem.ncbi.nlm.nih.gov/compound/10461 (accessed 2023-02-04).

(3) PubChem. *Hydrogen Cyanide*. https://pubchem.ncbi.nlm.nih.gov/compound/768 (accessed 2024-09-21).

(4) National Center for Biotechnology Information. *PubChem Compound Summary for CID 10757, 2-Chloroacetophenone*. PubChem. https://pubchem.ncbi.nlm.nih.gov/compound/10757 (accessed 2024-09-21).

(5) National Center for Biotechnology Information. *PubChem Compound Summary for CID 17604, 2-Chlorobenzylidenemalononitrile.* https://pubchem.ncbi.nlm.nih.gov/compound/17604 (accessed 2024-09-21).

(6) National Center for Biotechnology Information. *PubChem Compound Summary for CID 7871, Sarin.* PubChem. https://pubchem.ncbi.nlm.nih.gov/compound/7871 (accessed 2023-02-04).

(7) National Center for Biotechnology Information. *PubChem Compound Summary for CID 171040027, Novichok A-230.* https://pubchem.ncbi.nlm.nih.gov/compound/171040027 (accessed 2024-09-21).

(8) National Center for Biotechnology Information. *PubChem Compound Summary for CID 157299938, Novichok A-232.* https://pubchem.ncbi.nlm.nih.gov/compound/157299938 (accessed 2024-09-21).

(9) National Center for Biotechnology Information. *PubChem Compound Summary for CID 139033607, Novichok A-234.* https://pubchem.ncbi.nlm.nih.gov/compound/139033607 (accessed 2024-09-21).

(10) OPCW. *What is a Chemical Weapon?*. OPCW. https://www.opcw.org/our-work/what-chemical-weapon (accessed 2025-05-16).

(11) Schwenk, M. Chemical Warfare Agents. Classes and Targets. *Toxicol. Lett.* **2018**, *293*, 253–263. https://doi.org/10.1016/j.toxlet.2017.11.040.

(12) National Center for Biotechnology Information. *Lewisite*. PubChem Compound Summary for CID 5372798. https://pubchem.ncbi.nlm.nih.gov/compound/5372798 (accessed 2025-05-16).

(13) National Center for Biotechnology Information. *PubChem Compound Summary for CID 23969, Arsine*. PubChem Compound Summary for CID 23969, Arsine. https://pubchem.ncbi.nlm.nih.gov/compound/23969 (accessed 2025-05-16).

(14) Nancy B. Munro; Kathleen R. Ambrose; Annetta P. Watson. Toxicity of the Organophosphate Chemical Warfare Agents GA, GB, and VX: Implications for Public Protection. *Environ. Health Perspect.* **1994**, *102* (1), 18–37. https://doi.org/10.1289/ehp.9410218.

(15) Grob, D. The Manifestations and Treatment of Poisoning Due to Nerve Gas and Other Organic Phosphate Anticholinesterase Compounds. *Arch. Intern. Med.* **1956**, *98* (2), 221. https://doi.org/10.1001/archinte.1956.00250260095010.

(16) Clarke, S. F. J.; Chilcott, R. P.; Wilson, J. C.; Kamanyire, R.; Baker, D. J.; Hallett, A. Decontamination of Multiple Casualties Who Are Chemically Contaminated: A Challenge for Acute Hospitals. *Prehospital Disaster Med.* **2008**, *23* (2), 175–181. https://doi.org/10.1017/S1049023X00005811.

(17) Carlsen, L. After Salisbury Nerve Agents Revisited. *Mol. Inform.* **2019**, *38* (8–9), 1800106. https://doi.org/10.1002/minf.201800106.

(18) *Chemical Warfare Agents Biomedical and Psychological Effects, Medical Countermeasures, and Emergency Response*, 3rd ed.; Lukey, B. J., Romano, Jr., J. A., Salem, H., Eds.; CRC Press: Boca Raton, FL, USA, 2019.

(19) Szinicz, L. History of Chemical and Biological Warfare Agents. *Toxicology* **2005**, *214* (3), 167–181. https://doi.org/10.1016/j.tox.2005.06.011.

(20) Jones, M. R. 17: Personal Protective Equipment (PPE): Practical and Theoretical Considerations. In *Chemical Warfare Agents: Biomedical and Psychological Effects, Medical Countermeasures, and Emergency Response*; Salem, B. J. L., James A. Romano Jr ,. Harry, Ed.; CRC Press: Boca Raton, 2019. https://doi.org/10.1201/9781498769235.

(21) Canadian War Museum. *Weapons on Land - Poison Gas*. Canada and the First World War. https://www.warmuseum.ca/firstworldwar/history/battles-and-fighting/weapons-on-land/poison-gas/ (accessed 2023-06-16).

(22) Frederic J. Brown. *Chemical Warfare: A Study in Restraints*; Routledge: New York, 2017. https://doi.org/10.4324/9781315081472.

(23) Watson, A.; Opresko, D.; Young, R. A.; Hauschild, V.; King, J.; Bakshi, K. Chapter 9 - Organophosphate Nerve Agents. In *Handbook of Toxicology of Chemical Warfare Agents (Second Edition)*; Gupta, R. C., Ed.; Academic Press: Boston, 2015; pp 87–109. https://doi.org/10.1016/B978-0-12-800159-2.00009-9.

(24) Metcalf (deceased), R. L.; Horowitz, A. R. Insect Control, 2. Individual Insecticides. In *Ullmann's Encyclopedia of Industrial Chemistry*; John Wiley & Sons, Ltd, 2014; pp 1–94. https://doi.org/10.1002/14356007.s14_s01.

(25) Ganesan, K.; Raza, S. K.; Vijayaraghavan, R. Chemical Warfare Agents. *J. Pharm. Bioallied Sci.* **2010**, *2* (3), 166–178. https://doi.org/10.4103/0975-7406.68498.

(26) Oudejans, L. Persistence of Chemical Warfare Agent VX on Building Material Surfaces, 2019. https://cfpub.epa.gov/si/si_public_record_report.cfm?Lab=NHSRC&dirEntryId=345563 (accessed 2022-10-04).

(27) OPCW. *OPCW identifies ISIL as perpetrators of 2015 chemical attack in Marea, Syria*. OPCW. https://www.opcw.org/media-centre/news/2024/02/opcw-identifies-isil-perpetrators-2015-chemical-attack-marea-syria (accessed 2024-08-08).

(28) Hummel, K. *The Evolution of the Islamic State's Chemical Weapons Efforts*. Combating Terrorism Center at West Point. https://ctc.westpoint.edu/the-evolution-of-the-islamic-states-chemical-weapons-efforts/ (accessed 2024-08-08).

(29) OPCW. *History*. OPCW. https://www.opcw.org/about-us/history (accessed 2024-09-17).

(30) OPCW. *OPCW by the Numbers*. OPCW. https://www.opcw.org/media-centre/opcw-numbers (accessed 2024-09-17).

(31) Holmes, O.; Phillips, T. Kim Jong-Nam Killed by VX Nerve Agent, Say Malaysian Police. *The Guardian*. February 24, 2017. https://www.theguardian.com/world/2017/feb/24/kim-jong-nam-north-korea-killed-chemical-weapon-nerve-agent-mass-destruction-malaysian-police (accessed 2024-08-08).

(32) OPCW. *Report on the Use of a Chemical Weapon in the Death of a DPRK National*; OPCW, 2017; p 2. https://www.opcw.org/sites/default/files/documents/EC/84/en/Malaysia_ec84_statement.pdf (accessed 2023-01-19).

(33) Pak, J. H. *The education of Kim Jong-un*. Brookings. https://www.brookings.edu/articles/the-education-of-kim-jong-un/ (accessed 2024-08-08).

(34) John, H.; van der Schans, M. J.; Koller, M.; Spruit, H. E. T.; Worek, F.; Thiermann, H.; Noort, D. Fatal Sarin Poisoning in Syria 2013: Forensic Verification within an International Laboratory Network. *Forensic Toxicol.* **2018**, *36* (1), 61–71. https://doi.org/10.1007/s11419-017-0376-7.

(35) OPCW. *OPCW issues Fact-Finding Mission report on chemical weapons use allegation in Kafr Zeita, Syria, on 1 October 2016*. OPCW. https://www.opcw.org/media-centre/news/2022/02/opcw-issues-fact-finding-mission-report-chemical-weapons-use-allegation (accessed 2023-01-19).

(36) OPCW. *Report Of The OPCW On The Implementation Of The Convention On The Prohibition Of The Development, Production, Stockpiling And Use Of Chemical Weapons And On Their Destruction In 2017*; Reports of the OPCW on the Implementation of the Chemical Weapons Convention; Annual Report; OPCW: Den Hague, 2018; p 62.

https://www.opcw.org/sites/default/files/documents/2018/11/c2304%28e%29.pdf (accessed 2022-12-04).

(37) OPCW. *Report Of The OPCW On The Implementation Of The Convention On The Prohibition Of The Development, Production, Stockpiling And Use Of Chemical Weapons And On Their Destruction In 2018*; Reports of the OPCW on the Implementation of the Chemical Weapons Convention; Annual Report; OPCW: Den Hague, 2019; p 66. https://www.opcw.org/sites/default/files/documents/2019/12/c2404%28e%29.pdf (accessed 2022-12-04).

(38) Cofman Wittes, T.; Doran, M.; Byman, D. L.; Hamid, S.; Riedel, B. *Syria, the U.S., and Arming the Rebels: Assad's Use of Chemical Weapons and Obama's Red Line*. Brookings. https://www.brookings.edu/blog/up-front/2013/06/14/syria-the-u-s-and-arming-the-rebels-assads-use-of-chemical-weapons-and-obamas-red-line/ (accessed 2023-01-19).

(39) United Nations. *Syria: Grim 10-year anniversary of 'unimaginable violence and indignities' | UN News*. https://news.un.org/en/story/2021/03/1087402 (accessed 2024-08-28).

(40) Dawn Sturgess Inquiry. *The Dawn Sturgess Inquiry – Inquiry into 2018 Salisbury poisonings*. Dawn Sturgess Inquiry. https://www.dawnsturgess.independent-inquiry.uk/ (accessed 2023-02-28).

(41) Counter Terrorism Policing. *Salisbury & Amesbury Investigation*. Counter Terrorism Policing. https://www.counterterrorism.police.uk/salisbury/ (accessed 2024-11-23).

(42) Government of the United Kingdom. *Novichok nerve agent use in Salisbury: UK government response, March to April 2018*. GOV.UK. https://www.gov.uk/government/news/novichok-nerve-agent-use-in-salisbury-uk-government-response (accessed 2023-02-28).

(43) Government of the United Kingdom. *Clean-up work underway in Salisbury in next phase of recovery*. GOV.UK. https://www.gov.uk/government/news/clean-up-work-underway-in-salisbury-in-next-phase-of-recovery (accessed 2023-02-28).

(44) Haslam, J. D.; Russell, P.; Hill, S.; Emmett, S. R.; Blain, P. G. Chemical, Biological, Radiological, and Nuclear Mass Casualty Medicine: A Review of Lessons from the Salisbury and Amesbury Novichok Nerve Agent Incidents. *Br. J. Anaesth.* **2022**, *128* (2), e200–e205. https://doi.org/10.1016/j.bja.2021.10.008.

(45) Morris, S. Salisbury Inquiry: Novichok Bottle May Have Been 'Re-Sealed' after Poisoning. *The Guardian*. November 19, 2024. https://www.theguardian.com/uk-news/2024/nov/19/salisbury-inquiry-novichok-bottle-may-have-been-re-sealed-after-poisoning (accessed 2024-11-23).

(46) Gecsoyler, S. Ex-Police Officer Tells Sturgess Inquiry of Hallucinations after Novichok Poisoning. *The Guardian*. November 7, 2024. https://www.theguardian.com/uk-news/2024/nov/07/ex-police-officer-tells-sturgess-inquiry-of-hallucinations-after-novichok-poisoning (accessed 2024-11-23).

(47) Chai, P. R.; Hayes, B. D.; Erickson, T. B.; Boyer, E. W. Novichok Agents: A Historical, Current, and Toxicological Perspective. *Toxicol. Commun.* **2018**, *2* (1), 45–48. https://doi.org/10.1080/24734306.2018.1475151.

(48) Vale, J. A.; Marrs OBE, T. C.; Maynard CBE, R. L. Novichok: A Murderous Nerve Agent Attack in the UK. *Clin. Toxicol.* **2018**, *56* (11), 1093–1097. https://doi.org/10.1080/15563650.2018.1469759.

(49) Bellingcat Investigation Team. *The GRU Globetrotters: Mission London*. Bellingcat. https://www.bellingcat.com/news/uk-and-europe/2019/06/28/the-gru-globetrotters-mission-london/ (accessed 2024-09-07).

(50) Grozev, C.; van Huis, P.; Toler, A.; Tsalov, Y. *Navalny Poison Squad Implicated in Murders of Three Russian Activists*. Bellingcat. https://www.bellingcat.com/news/uk-and-europe/2021/01/27/navalny-poison-squad-implicated-in-murders-of-three-russian-activists/ (accessed 2024-09-07).

(51) OPCW. *Note by the Technical Secretariat Correspondence from Germany to the OPCW Requesting Technical Assistance in the Case of Mr. Alexei Navalny, and Associated Documents*; OPCW, 3 Aug 21. https://www.opcw.org/sites/default/files/documents/2021/08/s-1979-2021%28e%29.pdf (accessed 2024-09-07).

(52) Team, B. I. *"If it Hadn't Been for the Prompt Work of the Medics": FSB Officer Inadvertently Confesses Murder Plot to Navalny*. bellingcat. https://www.bellingcat.com/news/uk-and-europe/2020/12/21/if-it-hadnt-been-for-the-prompt-work-of-the-medics-fsb-officer-inadvertently-confesses-murder-plot-to-navalny/ (accessed 2023-01-19).

(53) Noga, M.; Jurowski, K. What Do We Currently Know about Novichoks? The State of the Art. *Arch. Toxicol.* **2022**. https://doi.org/10.1007/s00204-022-03437-5.

(54) Kaszeta, D. *A Guide to Cholinesterase Inhibitors in Wake of Suspected Alexei Navalny Poisoning*. Bellingcat. https://www.bellingcat.com/resources/2020/08/28/cholinesterase-inhibitors-alexei-navalny/ (accessed 2024-09-07).

(55) Team, B. I. *Russia's Clandestine Chemical Weapons Programme and the GRU's Unit 29155*. Bellingcat. https://www.bellingcat.com/news/uk-and-europe/2020/10/23/russias-clandestine-chemical-weapons-programme-and-the-grus-unit-21955/ (accessed 2024-09-07).

(56) Banaee, S.; Hee, S. S. Q. Glove Permeation of Chemicals: The State of the Art of Current Practice, Part 1: Basics and the Permeation Standards. *J. Occup. Environ. Hyg.* **2019**, *16* (12), 827–839. https://doi.org/10.1080/15459624.2019.1678754.

(57) US Army. *Test Operations Procedure (TOP) 08-2-501A, Permeation Testing of Materials With Chemical Agents or Simulants (Swatch Testing)*; Final TOP 08-2-501A; U.S. Army Dugway Proving Ground: Dugway, UT 84022-5000, 2013. https://apps.dtic.mil/sti/pdfs/ADA586844.pdf (accessed 2023-03-19).

(58) Rivin, D.; Lindsay, R. S.; Shuely, W. J.; Rodriguez, A. Liquid Permeation Through Nonporous Barrier Materials. *J. Membr. Sci.* **2005**, *246* (1), 39–47. https://doi.org/10.1016/j.memsci.2004.06.057.

(59) Frisch, H. L. The Time Lag in Diffusion. *J. Phys. Chem.* **1957**, *61* (1), 93–95. https://doi.org/10.1021/j150547a018.

(60) Rutherford, S. W.; Do, D. D. Review of Time Lag Permeation Technique as a Method for Characterisation of Porous Media and Membranes. *Adsorption* **1997**, *3* (4), 283–312. https://doi.org/10.1007/BF01653631.

(61) Fuoco, A.; Monteleone, M.; Esposito, E.; Bruno, R.; Ferrando-Soria, J.; Pardo, E.; Armentano, D.; Jansen, J. C. Gas Transport in Mixed Matrix Membranes: Two Methods for Time Lag Determination. *Computation* **2020**, *8* (2), 28. https://doi.org/10.3390/computation8020028.

(62) Paul, D. R. The Solution-Diffusion Model for Swollen Membranes. *Sep. Purif. Methods* **1976**, *5* (1), 33–50. https://doi.org/10.1080/03602547608066047.

(63) Baker, R. W. *Membrane Technology and Applications*, 3rd ed.; John Wiley & Sons, Ltd: Chichester, West Sussex, 2012. https://doi.org/10.1002/9781118359686.

(64) Geankoplis, C. J. *Transport Processes and Separation Process Principles (Includes Unit Operations)*, 4th ed.; Prentice Hall PTR: Upper Saddle River, NJ, 2003.

(65) Dickson, E. F. G. *Personal Protective Equipment for Chemical, Biological, and Radiological Hazards: Design, Evaluation and Selection*, 1st ed.; John Wiley & Sons, Ltd, 2012. https://doi.org/10.1002/9781118422991.

(66) Daugherty, M. L.; Watson, A. P.; Vo-Dinh, T. Currently Available Permeability and Breakthrough Data Characterizing Chemical Warfare Agents and Their Simulants in Civilian Protective Clothing Mater. *J. Hazard. Mater.* **1992**, *30* (3), 243–267. https://doi.org/10.1016/0304-3894(92)87002-W.

(67) Government of Canada, C. C. for O. H. and S. *CCOHS: Chemical Protective Clothing - Glove Selection*. https://www.ccohs.ca/oshanswers/prevention/ppe/gloves.html (accessed 2023-06-14).

(68) *Materials Science of Membranes for Gas and Vapor Separation*, 1st ed.; Yampolskii, Y., Pinnau, I., Freeman, B., Eds.; John Wiley & Sons, Ltd: Chichester, West Sussex, England, 2006. https://doi.org/10.1002/047002903X.

(69) Burganos, V. N. Modeling and Simulation of Membrane Structure and Transport Properties. In *Fundamentals of Transport Phenomena in Membranes*; Elsevier B V, 2010.

(70) Franz, T. J. Percutaneous Absorption. On the Relevance of in Vitro Data. *J. Invest. Dermatol.* **1975**, *64* (3), 190–195. https://doi.org/10.1111/1523-1747.ep12533356.

(71) Mellstrom, G. A. Comparison Of Chemical Permeation Data Obtained With Astm And Iso Permeation Test Cells—I. The Astm Standard Test Procedure. *Ann. Occup. Hyg.* **1991**. https://doi.org/10.1093/annhyg/35.2.153.

(72) Thibault, J.; Bergeron, S.; Bonin, H. W. On Finite-Difference Solutions Of The Heat Equation In Spherical Coordinates. *Numer. Heat Transf.* **1987**, *12* (4), 457–474. https://doi.org/10.1080/10407788708913597.

(73) Wu, H.; Al-Qasas, N.; Kruczek, B.; Thibault, J. Simulation of Time-Lag Permeation Experiments Using Finite Differences. *J. Fluid Flow Heat Mass Transf.* **2015**, *2*. https://doi.org/10.11159/jffhmt.2015.003.

(74) Ouvry. *CBRN Butyl gloves OG07*®. Ouvry - CBRN Protective System. https://ouvry.com/en/produit/cbrn-butyl-gloves/ (accessed 2023-05-09).

(75) Phalen, R. N.; Wong, W. K. Chemical Resistance of Disposable Nitrile Gloves Exposed to Simulated Movement. *J. Occup. Environ. Hyg.* **2012**, *9* (11), 630–639. https://doi.org/10.1080/15459624.2012.723584.

(76) Kimberly Clark Professional. *KleenGuard™ G10 Flex Nitrile Gloves (54333) - M Packaging, 100 Gloves / Box, 10 Boxes / Case, 1000 Gloves / Case*. KC Professional. https://www.kcprofessional.com/en-ca/products/safety-and-personal-protection-equipment/hand-protection-and-gloves/general-purpose-gloves/54331/54333 (accessed 2023-05-09).

(77) Lee, J.; Kim, E.-Y.; Chang, B.-J.; Han, M.; Lee, P.-S.; Moon, S.-Y. Mixed-Matrix Membrane Reactors for the Destruction of Toxic Chemicals. *J. Membr. Sci.* **2020**, *605*, 112–118. https://doi.org/10.1016/j.memsci.2020.118112.

(78) Motamedhashemi, M. M. Y.; Monji, M.; Egolfopoulos, F.; Theodore, T. A Hybrid Catalytic Membrane Reactor for Destruction of a Chemical Warfare Simulant. *J. Membr. Sci.* **2015**, *473*, 1–7. http://dx.doi.org/10.1016/j.memsci.2014.08.043.

(79) *MOF–Polymer Mixed Matrix Membranes as Chemical Protective Layers for Solid-Phase Detoxification of Toxic Organophosphates - University of Ottawa*. https://ocul-uo.primo.exlibrisgroup.com/discovery/fulldisplay?docid=cdi_pubmed_primary_36602325&context=PC&vid=01OCUL_UO:UO_DEFAULT&lang=en&search_scope=OCULDiscoveryNetworkNew&adaptor=Primo%20Central&tab=OCULDiscoveryNetwork&query=any,contains,MOF%E2%88%92Polymer%20Mixed%20Matrix%20Membranes%20as%20Chemical%20Protective%20Layers%20for%20Solid-Phase%20Detoxification%20of%20Toxic%20Organophosphates&offset=0 (accessed 2025-02-04).

(80) Cybenko, G. Approximation by Superpositions of a Sigmoidal Function. *Math. Control Signals Syst.* **1989**, *2* (4), 303–314. https://doi.org/10.1007/BF02551274.

(81) Wu, H.; Thibault, J.; Kruczek, B. The Validity of the Time-Lag Method for the Characterization of Mixed-Matrix Membranes. *J. Membr. Sci.* **2021**, *618*, 118715. https://doi.org/10.1016/j.memsci.2020.118715.

(82) Marquardt, D. W. An Algorithm for Least-Squares Estimation of Nonlinear Parameters. *J. Soc. Ind. Appl. Math.* **1963**, *11* (2), 431–441.

(83) Pal, T.; Griffin, G. D.; Miller, G. H.; Watson, A. P.; Daugherty, M. L.; Vo-Dinh, T. Permeation Measurements of Chemical Agent Simulants through Protective Clothing Materials. *J. Hazard. Mater.* **1993**, *33* (1), 123–141. https://doi.org/10.1016/0304-3894(93)85067-O.

(84) Duncan, S.; Mikler, J.; Lepage, C. J.; Clewley, R. *Responding to an Incident Involving Organophosphorus Nerve Agents*; Safety advisory and guidance DRDC-RDDC-2021-D106; DRDC: Ralston, AB, 2021; p 30.

(85) Dubey, V.; Gupta, A. K.; Maiti, S. N.; Rao, N. B. S. N. Diffusion and Sorption of Sulfur Mustard and Bis(2-Chloroethyl)Ether in Elastomers: A Comparative Study. *J. Appl. Polym. Sci.* **2000**, *77* (11), 2472–2479. https://doi.org/10.1002/1097-4628(20000912)77:11<2472::AID-APP16>3.0.CO;2-X.